Chapter 1
Introduction of Stimuli-Responsive Wetting/Dewetting Smart Surfaces and Interfaces

Gary J. Dunderdale and Atsushi Hozumi

Abstract Functional surfaces and interfaces possessing wetting/dewetting properties which change reversibly and repeatably in response to various external stimuli have attracted considerable attention lately because of their great potential in a wide variety of engineering fields, practical applications, and basic research. Different types of these smart surfaces/interfaces, on which chemical compositions and/or surface structures can be arbitrarily controlled by different external stimuli, such as pH, temperature, light, solvent, mechanical stress, electric/magnetic fields and so on, have been successfully prepared by various methods. This chapter will give an introduction to the basic theories of surface wetting/dewetting properties, including static/dynamic contact angles (CAs), CA hysteresis, Young's, Wenzel's, and Cassie-Baxter's equations, and in addition, typical examples and applications of stimuli-responsive wetting/dewetting smart surfaces and interfaces are also described.

Keywords Static/dynamic contact angles (CAs) · CA hysteresis · Young's, Wenzel's, and Cassie-Baxter's equations · Stimuli responsive · Wetting/dewetting

1.1 Introduction

The adherence of liquid droplets to solid surfaces can lead to corrosion, deterioration, reduction of visibility, and degradation of appearance, and thereby significantly damage the safety and reliability of everyday devices and industrial equipment. For this reason, the development of surface modifications that show excellent performance in liquid removal is of high importance, with extensive

G. J. Dunderdale
Department of Chemistry, University of Sheffield, Sheffield, UK

National Institute of Advanced Industrial Science and Technology (AIST), Nagoya, Japan

A. Hozumi (✉)
National Institute of Advanced Industrial Science and Technology (AIST), Nagoya, Japan
e-mail: a.hozumi@aist.go.jp

© Springer International Publishing AG, part of Springer Nature 2018

A. Hozumi et al. (eds.), *Stimuli-Responsive Dewetting/Wetting Smart Surfaces and Interfaces*, Biologically-Inspired Systems 11,
https://doi.org/10.1007/978-3-319-92654-4_1

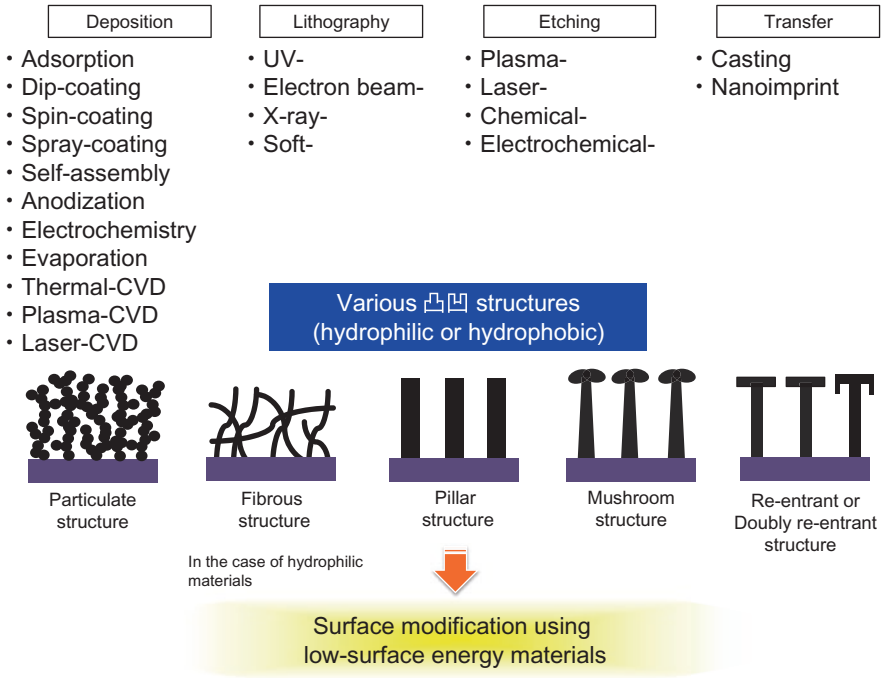

Fig. 1.1 Micro-/nano-fabrication methods and typical surface structures produced in the fabrication of man-made SLR surfaces

research on the control of adhesion and dewetting of liquid drops from solid surfaces having been reported so far. Most studies related to this research field have particularly focused on the effects of surface structures and chemical compositions on the surface wetting/dewetting properties (Onda et al. 1996; Hozumi and Takai 1997; Crevoisier et al. 1999; Chen et al. 1999; Lafuma and Qéré 2003; Gao and McCarthy 2006a; Tian et al. 2014). Many researchers have taken inspiration from Nature to achieve "superhydrophobic" surfaces, which generally display extremely large static contact angles (CAs, θ_S, greater than 150°), including lotus leaf surface and water strider's leg. Water droplets on such surfaces are unstable and can be easily moved, and needing the surface to tilt to only a small angle (low substrate tilt angles (θ_T) of less than 5~10°) before the drop rolls off. According to the Web of science®, the total number of papers of superhydrophobic surfaces is closing to 10,000 (Topic:"superhydrophobic" and "ultrahydrophobic") and more than 1000 papers have been published each year. In contrast to such skyrocketing publications on water-repellent surfaces, preparation of superoleophobic surfaces, where droplets of low-surface tension (γ) liquids such as oils can easily roll across and off the surface (exhibiting minimum θ_T for droplet motion of less than 5–10°), are rare (Tsujii et al. 1997; Tuteja et al. 2007; Zhang and Seeger 2011; Deng et al. 2012; Pan et al. 2013; Wang and Bhushan 2015; Brown and Bhushan 2016), in spite of the practical advantages they offer. In this chapter, we hereafter refer to the surfaces

possessing excellent liquid-repellent properties against various kinds of liquids as super-liquid-repellent (SLR) surfaces. Such man-made SLR surfaces have been generally prepared using a variety of techniques (Fig. 1.1) (Bhushan and Jung 2011) which commonly create micro/nano hierarchical structures, which are then subsequently treated using low-surface-energy materials (for example, terminated with alkyl or perfluoroalkyl groups).

In addition to such SLR surfaces which show high θ_S values, more recently, dynamic rather than static surface wetting/dewetting properties, which can be triggered by various external stimuli, including temperature, pH, magnetic/electric fields, solvents, light exposure and so on, has also attracted much attention due to their applications in a variety of engineering fields, such as oil/water separation (Kota et al. 2012; Dunderdale et al. 2015), drug delivery (Kim et al. 2013; Qiu and Park 2001), cell encapsulation (Kim et al. 2012), microfluidic devices (Huber et al. 2003), and so on (Sun and Qing 2011). Several important review papers on the topic of stimuli-responsive surfaces and interfaces have also been reported (Lahann et al. 2003; Feng and Jiang 2006; Xia et al. 2009; Xin and Hao 2010; Guo and Guo 2016).

In this chapter, we will describe basic theories of surface wetting/dewetting properties, including static/dynamic CAs, CA hysteresis, Young's, Wenzel's, and Cassie-Baxter's equations. In addition, typical examples and applications of stimuli-responsive wetting/dewetting smart surfaces and interfaces are also described.

1.2 Fundamental Theories of Surface Wetting/Dewetting

1.2.1 Flat/Smooth Surface

It is well-known that when a liquid droplet is placed on a solid surface, it tends to form a dome shape with a certain CA, rather than fully spreading out across the surface to form a thin film. In such a case, an apparent CA can be measured between the horizontal surface and the tangential line of the liquid surface near the three-phase (liquid (L), vapor (V), and solid (S) phases) contact line (Fig. 1.2). This apparent CA (θ_S) of a liquid on a smooth/flat surface can be estimated by Young's equation Eq. (1.1).

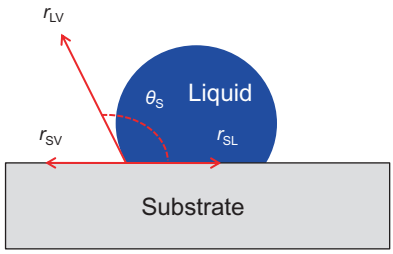

Fig. 1.2 Liquid droplet placed on a smooth/flat surface and vector representation of the three-surface tensions (γ_{LV}, γ_{SV}, and γ_{SL}) interacting on the liquid droplet

$$\cos\theta_S = \left(\gamma_{SV} - \gamma_{SL}\right)/\gamma_{LV} \tag{1.1}$$

γ_{LV}: surface tension at the L-V interface, γ_{SV}: surface tension at the S-V interface, and γ_{SL}: surface tension at the S-L interface.

A surface with a θ_S value of less than 90° is regarded as hydrophilic/oleophilic, and in particular when θ_S is close to 0°, it is called a superhydrophilic/superoleophilic surface. In contrast, a surface with a θ_S value of over 90° is regarded as hydrophobic/oleophobic, and when this value becomes larger than 150°, superhydrophobic/superoleophobic.

Superhydrophobic surfaces generally exhibit excellent liquid repellency due to the small area of contact between the drop and the surface caused by the high CA. However, there are adhesive/sticky surfaces on which water drops remain pinned to the surface regardless of the magnitude of their θ_S values (Jin et al. 2005). Rose petal surfaces are a good example; they exhibit 'superhydrophobicity', but at the same time are strongly adhesive towards water (so called "rose-petal effect") (Jin et al. 2005). In addition, such "pinning" phenomena have also been frequently observed on conventional hydrophobic glass windows and car windshields with water θ_S values of ~120°, as can be seen on rainy days even if the surface has been treated with perfluoroalkylsilanes. As is obvious from this example, it is clear that surface dewetting properties cannot be characterized by θ_S values alone, which have conventionally been used to explain this behavior. Thus, recently, to accurately characterize surface wetting/dewetting properties, measurements of dynamic wettability, advancing (θ_A) and receding (θ_R) CAs, CA hysteresis, and θ_T, have been used (Cheng et al. 2012a, b; Wong et al. 2013). Hereafter we will explain these measurements and use them to explain observed phenomena.

CA hysteresis is the mass-independent measure of the resistance to macroscopic liquid drop movement on inclined surfaces. It recognizes that in order for the gravitational force to cause a liquid drop to de-pin from a stationary position on a horizontal surface and begin sliding/rolling down an inclined surface, the shape of the liquid drop must first undergo a certain amount of deformation, as shown in Fig. 1.3.

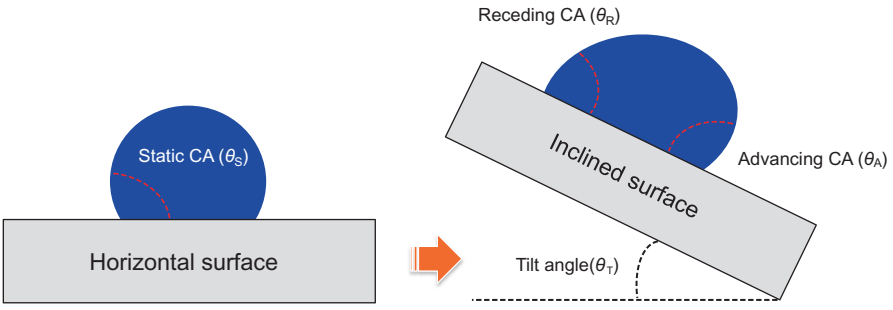

Fig. 1.3 Comparison of liquid drops on horizontal (left) and inclined (right) surfaces. The advancing CA (θ_A) indicates the maximum angle just before the droplet advances. The receding CA (θ_R) indicates the minimum angle just before the droplet recedes

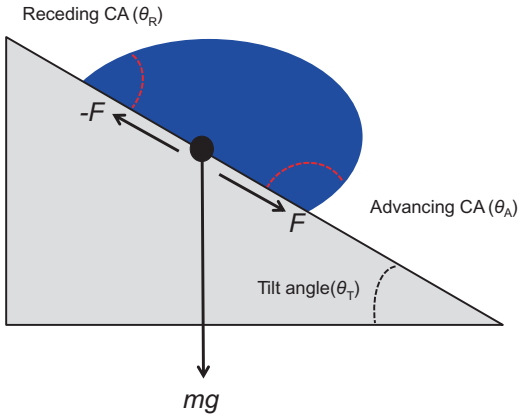

Fig. 1.4 Liquid droplet on an inclined surface. The substrate tilt angle (θ_T) indicates the angle at which the gravitational force ($F = mg \bullet \sin \alpha$) overcomes the lateral adhesion force ($-F$) and induces sliding/rolling of the liquid droplet

Assuming that the solid-liquid contact area remains constant or experiences a relatively insignificant change, this deformation from its typical spherical dome/cap shape results in an increase in the drop's liquid-vapor interfacial area. The energy associated with this increase has been described as the activation energy barrier to liquid drop motion down an inclined surface (Gao and McCarthy 2006b, 2009). From the initial horizontal position (at θ_S), the drop begins to move when its CAs at the front and back ends are capable of advancing and receding, respectively. These advancing and receding events, which occur at θ_A and θ_R, are also the maximum and minimum possible CAs, respectively, for a liquid-surface pair. CA hysteresis can be described using θ_A and θ_R, or the cosine of these values as follows:

$$\Delta\theta = \theta_A - \theta_R \tag{1.2}$$

$$\Delta\theta_{\cos} = \cos\theta_R - \cos\theta_A \tag{1.3}$$

Kawasaki and Furmidge reported that there is a relation between the mobility of probe liquids on an inclined surface and $\Delta\theta_{\cos}$ (=cosθ_R – cosθ_A) (Kawasaki 1960; Furmidge 1962). The gravitational force required to initiate drop movement across an inclined surface (Fig. 1.4) dependent on $\Delta\theta_{\cos}$ is described by Eq. (1.4).

$$F = mg \cdot \sin\theta_T = kw\gamma_{LV}\left(\cos\theta_R - \cos\theta_A\right) \tag{1.4}$$

m: the mass of the drop, g: the gravitational constant, α: substrate tilt angle (θ_T), k: constant that depends on drop shape, w: the width of the drop, and γ_{LV}: the L-V surface tension.

According to Eq. (1.4), $\Delta\theta_{\cos}$ (Eq. (1.3)) shows significantly stronger correlation with the resulting θ_T values of a liquid drop on a surface than with the conventional definition of CA hysteresis ($\Delta\theta$, Eq. (1.2)) (Cheng et al. 2012b). Therefore, when CA hysteresis value is small enough, a liquid drop will only require a low θ_T value to de-pin from a horizontal position and begin moving down the surface without

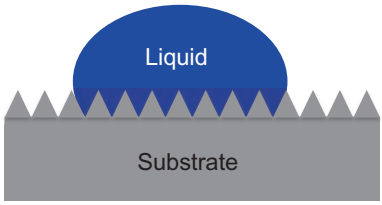

Fig. 1.5 Schematic illustration of the possible wetting state of liquid droplet placed on a chemically homogeneous rough surface (Wenzel state)

substantial deformation of its shape. Conversely, drops can remain permanently pinned to vertically oriented surfaces, regardless of their magnitude of θ_S values (even if the θ_S values are over 150°), when the CA hysteresis is significant. Actually, in many cases, the θ_S values of SLR surfaces were less influenced by surface contaminations and defects, but they have a serious influence on dynamic CAs (in particular, θ_R values decrease), affecting the sliding/rolling properties (Verho et al. 2011). Thus, the latest definition of SLR surfaces is that they display not only high θ_S values (greater than 150°), but also low $\Delta\theta$ values (less than 5–10°), and low θ_T values (less than 5–10°) for small volumes (3–5 μL) of various probe liquids, not only water but also virtually all probe liquids including low γ liquids (below 30 dyn/cm) (Kota et al. 2014).

1.2.2 Rough Surface

In contrast to flat/smooth surfaces, when a liquid droplet contacts a rough surface, it can adopt one of the following two configurations to minimize its overall free energy (Marmur 2003; Nosonovsky 2007), *i.e.,* the Wenzel (Wenzel 1936) or the Cassie-Baxter state (Cassie and Baxter 1944). As shown in Fig. 1.5, in the Wenzel state, the liquid droplet completely permeates into the voids on the rough surface underneath of the liquid droplet, forming a fully-wetted interface. As these voids are usually very small (<10 μm), it is not possible to measure the angle between the surface and the tangent of the liquid drop (CA) without the use of microscopy. In this case, an apparent CA is defined as the angle between the tangent of the liquid drop and the plane of the rough surface as viewed on a macroscopic scale. In this Wenzel state, this apparent CA (θ_W) is related to the real CA by Wenzel's equation Eq. (1.5) (Wenzel 1936).

$$\cos\theta_w = r \cdot \cos\theta \tag{1.5}$$

θ_W: Wenzel's CA on the rough surface, θ: CA on the smooth/flat surface of the identical material, r: the surface roughness factor (r = actual surface area/projected surface area).

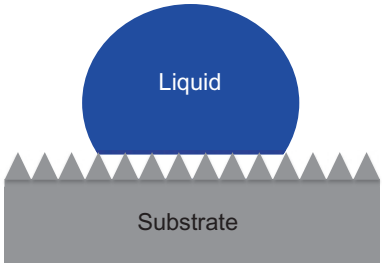

Fig. 1.6 Schematic illustration of the possible wetting state of liquid droplet placed on a chemically heterogeneous rough surface (Cassie-Baxter state)

In the Wenzel state, because r is always larger than 1, surface roughness amplifies both wetting/dewetting behaviors of materials. When the θ value is less than 90°, the θ_W value will decrease, while when the θ value is larger than 90°, the θ_W value will increase with an increase in surface roughness. However, actual droplets on the rough surfaces do not exhibit the apparent CAs (θ_W) described by Eq. (1.5), because the three-phase contact line of the liquid is frequently pinned to the surface by defects/voids from the production mechanism, resulting in an increase in CA hysteresis (Forsberg et al. 2010). The Wenzel model is also only applicable to chemically homogeneous rough surfaces, whereas in real life, many of the produced surfaces are heterogeneous.

In contrast, in the Cassie-Baxter state, when a liquid droplet is placed on a rough surface, the liquid doesn't flow into the voids of the surface, and they remain filled with air underneath the droplet, as can be seen in Fig. 1.6. Now the L-S interface is a composite interface consisting of two components, in this case, L-substrate and L-air. Moreover, the Cassie-Baxter state can also account for the effects of chemical heterogeneities of the rough surface on the apparent CA, if extra terms with different CAs are included in this composite interface. The general Cassie's equation is given by Eq. (1.6).

$$\cos\theta_C = f_1\left(\cos\theta_1\right) + f_2\left(\cos\theta_2\right) \tag{1.6}$$

θ_C: Cassie's CA of the rough surface, f_1 and f_2 are the area fractions, and θ_1 and θ_2 are CA of the flat/smooth materials 1 and 2, respectively.

In Cassie–Baxter state, for example, when f_2 component is air, and $f_1 + f_2 = 1$, $\cos\theta_2$ (=cos180°) is −1, and $f_2 = 1 - f_1$, respectively. Thus, the apparent CA (θ_{CB}) is finally given by Cassie-Baxter's equation (Eq. 1.7) (Cassie and Baxter 1944).

$$\begin{aligned}\cos\theta_{CB} &= f_1\left(\cos\theta_1\right) - f_2 \\ &= f_1\left(\cos\theta_1\right) - \left(1 - f_1\right) \\ &= f_1\left(\cos\theta_1 + 1\right) - 1\end{aligned} \tag{1.7}$$

In contrast to the Wenzel state, high values of f_2 (air-area fraction) in the Cassie-Baxter state enhance the magnitude of the θ_{CB} values. In such a case, liquid droplet is unstable and can move smoothly without pinning on the surface.

1.3 Preparation Methods of Stimuli-Responsive Smart Surfaces and Interfaces

A wide variety of surface functionalization methods, such as electrospinning (Huang et al. 2013; Ma et al. 2016a; Wang et al. 2016a; Sarbatly et al. 2016; Tai et al. 2014; Obaid et al. 2015a; Ning et al. 2015; Ma et al. 2016b; Alayande et al. 2016; Zhang et al. 2015; Arslan et al. 2016; Obaid et al. 2015b; Fang et al. 2016; Liu and Liu 2016; Li et al. 2016a, b; Wang et al. 2015, 2016b; Che et al. 2015), surface-initiated atom-transfer radical polymerization (SI-ATRP) (Wang et al. 2015; Sun et al. 2004; Barbey et al. 2009; Jain et al. 2009; Matyjaszewski and Tsarevsky 2009; Koenig et al. 2014; Dunderdale et al. 2014), layer-by-layer (LBL) deposition (Yang et al. 2011a; Lu et al. 2013; Lim et al. 2006), self-assembly (self-assembled monolayers: SAMs) (Liu et al. 2013; Jin et al. 2011), spray-deposition (Yang et al. 2011b; Zhang et al. 2012), spin-coating (Li et al. 2009), electrodeposition (Xu et al. 2014), Langmuir-Blodgett (LB) methods (Feng et al. 2001), electrochemical deposition (Wang and Guo 2013) and so on (Wu et al. 2013; Byun et al. 2012; Wang and Zhang 2012), have been reported to prepare stimuli-responsive smart surfaces and interfaces.

Some typical examples of functionalized surfaces and interfaces showing stimuli-responsive properties are summarized in Table 1.1.

The electrospinning technique has become a versatile and effective method for synthesizing nanofibrous materials with controlled compositions and morphologies (Agarwal et al. 2013; Misra et al. 2017; Ding et al. 2010; Singh et al. 2016). In addition, electrospinning can provide other important features, such as high surface-to-volume ratio and multi-porous structures possessing unique chemical, physical, and mechanical properties by incorporating other components with ease and control (Li and Xia 2004; Ramakrishna et al. 2006; Wang et al. 2013; Bhardwaj and Kundu 2010). Because of the highly specific surface areas, interconnected nano-scale pore structures, and the potential to incorporate active chemical functionality on a nano-scale surface, electrospinning is one of the promising and cost-effective methods to prepare stimuli-responsive smart surfaces and interfaces. Various polymeric membranes and nanofibrous mats showing stimuli-responsive properties have been successfully fabricated by this method and have been widely applied for oil/water separation applications (For example, Fig. 1.7) (Huang et al. 2013; Ma et al. 2016a; Wang et al. 2016a; Sarbatly et al. 2016; Tai et al. 2014; Obaid et al. 2015a; Ning et al. 2015; Ma et al. 2016b; Alayande et al. 2016; Zhang et al. 2015; Arslan et al. 2016; Obaid et al. 2015b; Fang et al. 2016; Liu and Liu 2016; Li et al. 2016a, b; Wang et al. 2015, 2016b; Che et al. 2015). Although electrospinning is a useful technique to prepare structured smart surfaces and interfaces, the resulting structures and properties of electrospun nanofibers are considerably influenced by experimental factors, such as molecular weight (MW) and solubility of polymers, the solvent/solution properties, and external environmental conditions (Doshi and Reneker 1995; Megelski et al. 2002; Huang et al. 2003; Lee et al. 2003).

Table 1.1 Typical examples of functionalized surfaces and interfaces showing stimuli-responsive properties[a]

Stimuli	Substrate shape	Materials/chemicals	Preparation methods	References
Stress/ stretch	Film	PTFE	N.A.	Zhang et al. (2004)
		Polyamide		Zhang et al. (2005)
pH	Fiber mat	PBz	Electrospinning	Liu and Liu (2016)
	Cu mesh	Cu-NPs/Au/ $HS(CH_2)_9CH_3$ and $HS(CH_2)_{10}COOH$	Electrochemical deposition/ self-assembly	Wang and Guo (2013)
Temperature	Si micro-convexes	PNiPAAm	SI-ATRP	Xia et al. (2009)
	RC nanofibrous membrane			Wang et al. (2015)
Light	Nanofibrous membrane	TiO_2-NPs/PVDF	Electrospinning	Wang et al. (2016b)
	Si	CF_3AZO/PAH/SiO_2-NPs	LBL deposition	Lim et al. (2006)
Magnetic field	Ni-micronails	1*H*,1*H*,2*H*,2*H*-Perfluorodecanethiol	Electrodeposition/ self-assembly	Grigoryev et al. (2012)
	Structured Si	Fe_3O_4-NPs	N.A.	Cheng et al. (2012c)
Gas	Nanofibers	PMMA-*co*-PDEAEMA	Electrospinning	Che et al. (2015)
	SAM/Au	NADPA	Self-assembly/ grafting	Li et al. (2014b)
Solvent	Structured PTFE	PSF-COOH/PVP-COOH	Grafting	Minko et al. (2003)
	Structured Si	PNiPAAm-*co*-Cy&AA		Wang et al. (2009)

[a]Abbreviations: *PTFE* Polytetrafluoroethylene, *PBz* Polybenzoxazine, *NPs* Nanoparticles, *RC* regenerated cellulose, *PNiPAAm* Poly(*N*-isopropylacrylamide), *SI-ATRP* Surface-initiated atom-transfer radical polymerization, *PVDF* Polyvinylidene fluoride, *CF_3AZO* 7-[(trifluoromethoxyphenylazo) phenoxy]pentanoic acid, *PAH* Poly(allylamine hydrochloride), *LBL* Layer-by-layer, *PMMA-co-PDEAEMA* Poly(methyl methacrylate)-*co*-poly(*N,N*-diethylaminoethyl methacrylate), *NADPA* *N*-(2-aminoethyl)-5-(1,2-dithiolan-3-yl) pentanamide amidine, *PSF* Pentafluorostyrene, *PVP* Poly(*N*-vinylpyrrolidone), *PNiPAAm-co-Cy&AA* Aspartic acid (AA) and cysteine (Cy) units grafted PNiPAAm

SI-ATRP is a novel approach to fabricate stimuli-responsive smart surfaces and interfaces by growing low polydispersity polymer chains on a surface (Fu et al. 2004). Responsive polymer brushes prepared by SI-ATRP have recently attracted considerable attention because of their great potential for the preparation of stimuli-responsive surfaces (Sun et al. 2004; Barbey et al. 2009; Jain et al. 2009; Matyjaszewski and Tsarevsky 2009; Koenig et al. 2014; Dunderdale et al. 2014).

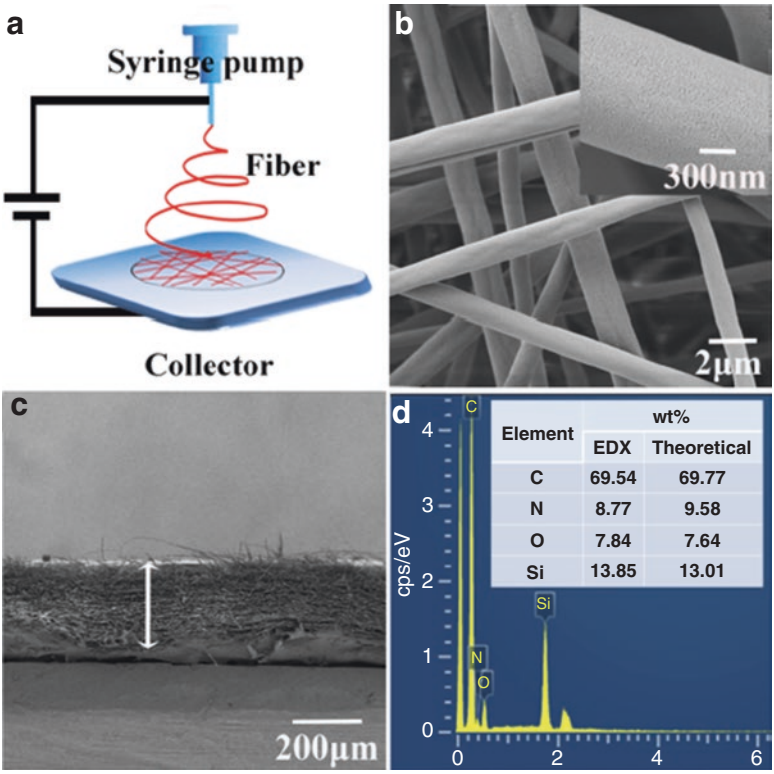

Fig. 1.7 (**a**) Schematic illustration of the electrospinning process. (**b**) Representative SEM image of pH-responsive polymer (PDMS-*b*-P4VP: poly(dimethylsiloxane)-*block*-poly(4-vinylpyridine)) fibers (inset is the zoomed-in image of the surface of a single fiber). (**c**) Cross-sectional morphology and (**d**) EDX spectrum of the polymer fibrous mat (inset table shows the element content obtained using EDX and theoretical calculations). (Reproduced with permission from (Li et al. 2016a), Copyright 2016 The American Chemical Society)

For example, a thermally-responsive poly(*N*-isopropylacrylamide) (PNiPAM) surface was reported by Sun et al. by growing polymers from flat and rough Si substrates using SI-ATRP (Sun et al. 2004). As shown in Fig. 1.8, the authors have fabricated poly(2-(dimethylamino)ethyl methacrylate) (PDMAEMA) polymer brush on a large-scale aluminum substrate (30×10 cm^2) in air by using a modified SI-ATRP, so-called SI-"Paint on"-ATRP. This surface shows switchable underwater oleophobicity depending on the solution pH (Dunderdale et al. 2014).

A very serious limitation of conventional SI-ATRP is that it typically requires high concentrations of monomer, and catalyst, use of organic solvents, elevated reaction temperatures, and the reaction solution to be rigorously purged of oxygen (Barbey et al. 2009). Such stringent conditions make it difficult to prepare smart stimuli-responsive surfaces and interfaces outside of laboratory conditions, and due to practical difficulties associated with the reaction setup, impractical for large area ($\sim$1 m^2) functionalization. To overcome these shortcomings, modified ATRP proto-

Fig. 1.8 Functionalization of large real life substrates. (Top) 1.3 L glass jar functionalized by low-chemical content SI-ATRP. Jars contain water adjusted to either pH 2 or pH 10 and *n*-hexane containing blue dye. At pH 2 the surface of the jar was superoleophobic, whereas at pH 10 oil drops adhered to the surface. (Bottom) Aluminum sheet functionalized using SI-"Paint on"-ATRP. (Reproduced with permission from (Dunderdale et al. 2014), Copyright 2014 The American Chemical Society)

cols, called Activators (Re)Generated by Electron Transfer (A(R)GET)-ATRP, water-accelerated ATRP, and SI-"Paint on"-ATRP, have been developed and proposed as solutions to these limitations (Dunderdale et al. 2014; Simakova et al. 2012; Jones and Huck 2001).

LBL deposition is also commonly used to control surface wetting/dewetting properties, which uses self assembly of polyelectrolytes or nanoparticles (NPs) with opposing charges to form smart responsive surfaces and interfaces.

For example, Yang et al. (2011a) prepared polyelectrolyte multilayer (PDDA: poly(diallyldimethylammonium chloride)/PSS: poly(sodium 4-styrene sulfonate), covered cotton fabrics by using LBL deposition. As shown in Fig. 1.9, the resulting surfaces showed switchable wettability between non-wetting (CAs of water and *n*-hexadecane were about 151°and 140°, respectively) and fully wetted state for both water and *n*-hexadecane drops. The stimuli-responsive behavior took advantage of counterion exchange between Cl^- and sodium perfluorooctanoate (PFO) anions to produce these changes in wettability. Lu et al. (2013) also prepared LBL hydrogel (amphiplilic polymers)-covered microstructured Si surfaces which showed controllable wettability through pH-induced reversible collapse/solubilization transitions in solution.

LBL deposition enables the inclusion of various polymers and different-sized NPs within the resulting multilayer thin film, which can be used to increase surface roughness or porosity (Lu et al. 2013; Li et al. 2014a). Other advantages of this technique are that the film structure and chemical composition can be easily controlled, and it can be applicable to large-area substrates of arbitrarily shape,

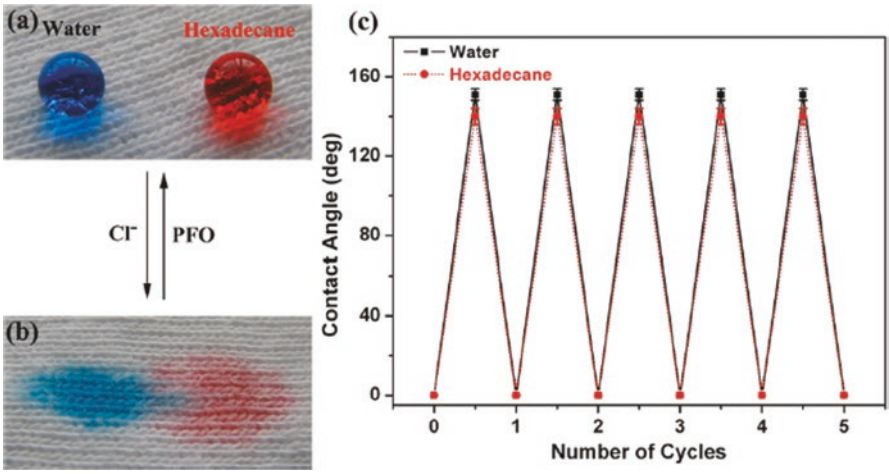

Fig. 1.9 (**a** and **b**) Water and *n*-hexadecane droplets on the polyelectrolyte-deposited cotton fabric surfaces coordinated with PFO anions and Cl^-, respectively. (**c**) Switchable superhydrophobicity and superoleophobicity of the polyelectrolyte-deposited fabric surfaces with water and *n*-hexadecane *via* consecutive counterion exchange. (Reproduced with permission from (Yang et al. 2011a), Copyright 2011 The American Chemical Society)

porosity, and chemistry (Decher 1997). In conflicting roles, the intermolecular binding between polymers, which ensures stability of LBL films, becomes a major obstacle to the formation of smart responsive surfaces and interfaces capable of switching their surface wetting properties (Guo and Guo 2016).

Other methods, such as self-assembly (Liu et al. 2013; Jin et al. 2011), spray-deposition (Yang et al. 2011b; Zhang et al. 2012), spin-coating (Li et al. 2009), electrodeposition (Xu et al. 2014), LB method (Feng et al. 2001), electrochemical deposition (Wang and Guo 2013) and so on (Wu et al. 2013; Byun et al. 2012; Wang and Zhang 2012), have also been reported to fabricate smart stimuli-responsive surfaces and interfaces. In spite of these methods offering attractive advantages, there are requirements for further improvement of the stability of the smart-responsive surfaces/interfaces prepared by these approaches before widespread use becomes practical.

1.4 Typical Stimuli-Responsive Smart Surfaces and Interfaces

1.4.1 Mechanical (Stress/Stretch) Response

As mentioned above, surface wettability/dewettability are governed by surface structures and chemical compositions. Thus, if either of these factors is reversibly manipulated, surface wettability/dewettability is also reversibly controlled. In most of the reported stimuli-responsive behavior, it is the chemical composition, which is

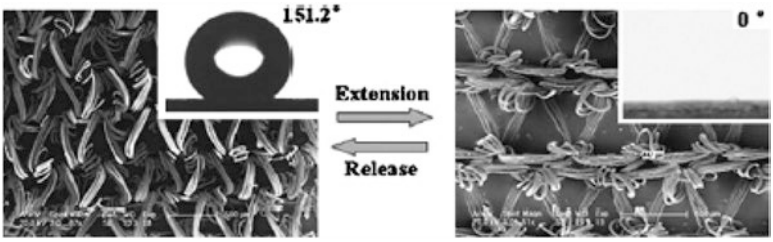

Fig. 1.10 Reversible change in surface structure and wettability of the triangular polyamide film with and without extension. (Reproduced with permission from (Xia et al. 2009), Copyright 2005 The Royal Society of Chemistry)

reversibly changed, however, changes in surface structures also cause changes in wettability/dewettability. There have been a few reports on stress-responsive smart surfaces and interfaces, which rely on this fact (Zhang et al. 2004, 2005; Lin and Yang 2009; Chung et al. 2007; Huang et al. 2015).

Zhang et al. (2004) reported a reversible wettability transition from hydrophobic to superhydrophobic of elastic poly(tetrafluoroethylene) (PTFE) films by stress stimulation. With an increase in the axial extension from 0 to 190%, water CAs increased from 108° to 165° because of the change in the density of the PTFE crystals during the axial extension. Zhang et al. (2005) also reported similar reversible wettability transitions in elastic polyamide films. When the film was bi-axially extended to more than 120%, the water droplet completely spread across the surface showing superhydrophilicity (Fig. 1.10, **right**), while after unloading, the surface returned to superhydrophobic again because of the recovery of surface microstructures (Fig. 1.10, **left**).

Similarly, PDMS films which have a wrinkled topography have shown to change their wettability when stretched. When not under mechanical strain the topography is highly wrinkled meaning that water drops sit on top of the surface in the Cassie-Baxter state, and can slide across the surface at an angle of ~15°. However, when mechanical strain is applied to this surface the wrinkled topography becomes less pronounced and it is harder for the drops to slide. On the same surface the sliding angle increased to ~50° when a mechanical strain of 40% was applied (Lin and Yang 2009). Chung et al. observed that CA's of water drops had only a single value when a PDMS film was smooth, but when compressed to form wrinkles had two different CA's depending on whether the orientation of the wrinkles was parallel or perpendicular to the observer. In this case the CA measured perpendicular to the wrinkles increased from ~65° to ~110° as the film was compressed to form wrinkles (Chung et al. 2007).

1.4.2 pH Response

pH-responsive materials have been widely applied to various fields, such as drug delivery, enzyme-immobilization, oil/water separation, chemo-mechanical system, chemical valves, and sensors (Xia et al. 2009).

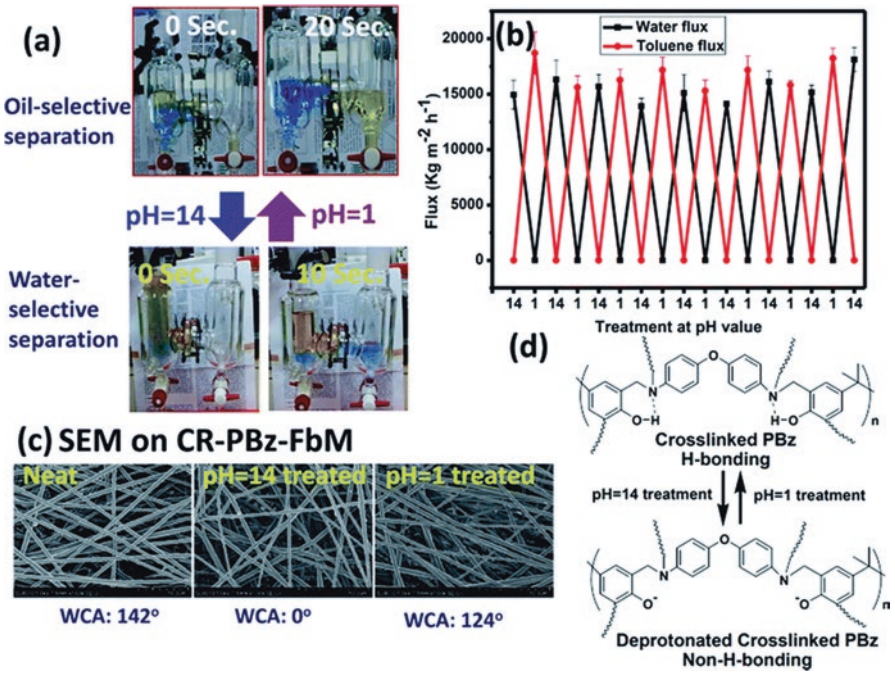

Fig. 1.11 (**a**) pH-induced switching of oil- and water-selectivity of the CR-PBz-FbM membrane in oil/water separation. (**b**) The membrane permeation fluxes in cycled treatment of the membrane with solutions of different pH values (pH 14 and pH 1). The changes in membrane selectivity are almost completely reversible without sacrificing the permeation fluxes. (**c**) SEM micrographs of the CR-PBz-FbM membrane treated with solutions of different pH values (pH 14 for 5 min and pH 1 for 1 min). (**d**) A scheme illustrating the changes in the chemical structure and hydrogen-bonding of CR-PBz-FbM being treated with solutions of different pH values (pH 14 and pH 1). Deprotonation of the crosslinked PBz structure results in loss of hydrogen bonding so as to turn the membrane from oleophilic to hydrophilic. (Reproduced with permission from (Liu and Liu 2016), Copyright 2016 The Royal Society of Chemistry)

For example, Liu and Liu (2016) prepared pH-responsive surfaces by electrospinning. Polybenzoxazine (PBz) was electrospun, and the collected PBz fiber mat then dried at 60 °C under vacuum, and finally cured thermally at 200 °C for 1 h and 240 °C for 3 h. The resulting cross-linked electrospun PBz fiber mat (CR-PBz-FbM) showed a hydrophobic nature. These mats were tested as potential pH-switchable oil/water separation meshes, as shown in Fig. 1.11. It was found that for solutions of pH 14, the mat showed oil-selective behavior, and at pH 1 it showed the opposite behavior being water-selective.

Huang et al. (2015) recently reported smart surfaces of hydrogels containing silanized glass particles showing reversible wettability from superhydrophobicity to superhydrophilicity under the different types of stimuli such as pH, temperature,

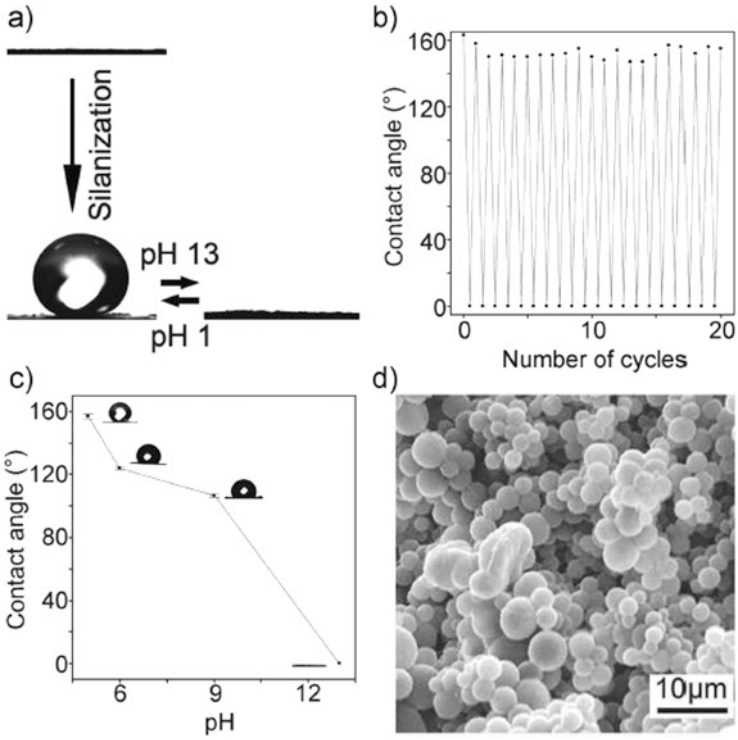

Fig. 1.12 Controlling the wettability of the pH-responsive composite material. (**a**) When the glass particles were not silanized, the water CA on the surface was 0°. After silanization, the surface became superhydrophobic (water CA was more than 150°). When the material was expanded by a solution of pH 13, the surface became superhydrophilic. (**b**) The switch from superhydrophobicity to superhydrophilicity was reversible as demonstrated by expanding and contracting the material in solutions of pH 13 and pH 1, respectively, for 20 times. (**c**) The water CA could be tuned by immersing the material in solutions of different pH. (**d**) An SEM image of the glass particles on the surface of the material (Reproduced with permission from (Huang et al. 2015), Copyright 2015 Wiley-VCH Verlag GmbH & Co. KGaA, Weinheim)

and stress. pH-responsive hydrogels were prepared by mixing acrylic acid, 2-hydroxyethyl methacrylate, ethylene glycol dimethacrylate (cross-linker), 2,2-dimethoxy-2-phenylacetophenone (photoinitiator), and deionized water. The mixture was then poured into the glass container covered with the layers of glass particles, and cured for a certain time. As shown in Fig. 1.12, after silanization using methyltrichlorosilane, the static water CA on the pH-responsive hydrogel surface was more than 150°. When the gel was immersed in a basic solution (pH 13), it expanded and became superhydrophilic, whereas by immersing it in an acidic solution (pH 1), it contracted and became superhydrophobic again, showing excellent tunable and reversible wettability.

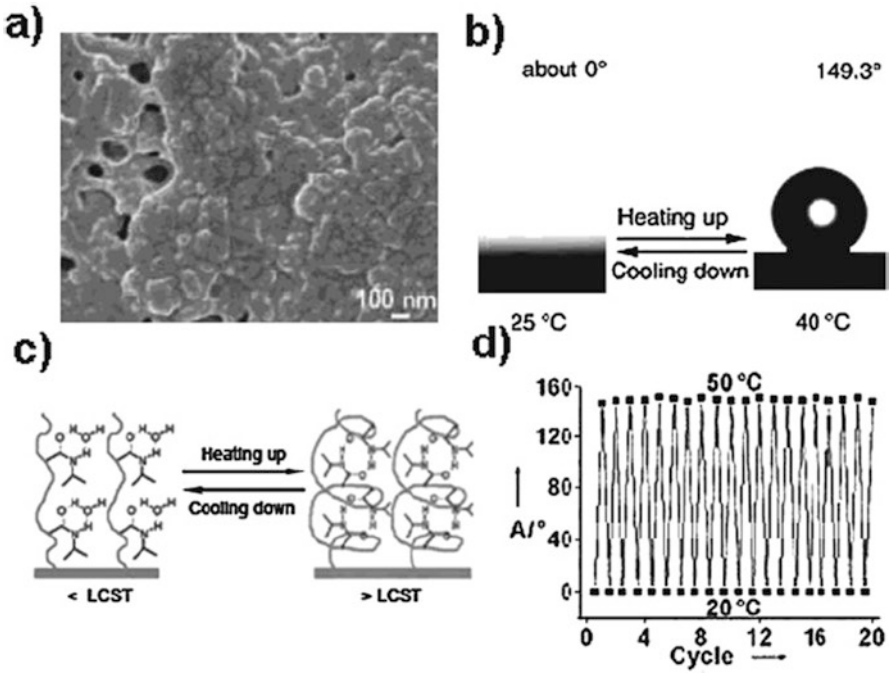

Fig. 1.13 (**a**) SEM image of the nanostructures on rough substrate modified with PNiPAAm. (**b**) Water drop profile for responsive surface at 25 °C and 40 °C. (**c**) Diagram of reversible formation of intermolecular hydrogen bonding between PNiPAAm chains and water molecules (left) and intramolecular hydrogen bonding between C=O and N–H groups in PNiPAAm chains (right) below and above the LCST, which is considered to be the molecular mechanism of the temperature-responsive wettability of a PNiPAAm thin film. (**d**) CAs at two different temperatures 20 °C and 40 °C for PNiPAAm-modified rough substrate. (Reproduced with permission from (Xia et al. 2009), Copyright 2009 The Royal Society of Chemistry)

1.4.3 Temperature Response

There have been numerous reports of materials which change their wettability in response to changes in temperature. Polymeric materials, which show a Lower Critical Solution Temperature (LCST), have been extensively used in this research field. For example, PNiPAAm is a typical temperature-responsive polymer that has a lower LCST of about 32–33 °C (Feng and Jiang 2006; Xia et al. 2009; Sun et al. 2004).

For example, Jiang's group (Xia et al. 2009; Sun et al. 2004) reported a smooth PNiPAAm surface exhibiting a controllable range of water CAs from 63.5° to 93.2°, *i.e.*, changing from slightly hydrophilic to slightly hydrophobic, as the temperature passed through the LCST. This is the result of the competition between intra- and intermolecular hydrogen bonding (Fig. 1.13c). On the other hand, when the PNiPAAm was deposited on a rough surface (Si microconvexes), the wettability

could be changed from 0° to 149.3° when the temperature was elevated from 25 °C to 40 °C, indicating reversible switching between superhydrophobicity and superhydrophilicity (Fig. 1.13b, d).

PNiPAAm-based polymers have been commonly used for the preparation of temperature-responsive surfaces (Li et al. 2016b; Wang et al. 2015; Sun et al. 2004; Koenig et al. 2014; Chen et al. 2010; Liu et al. 2015), along with other types of temperature-responsive materials as will be described below.

Yang et al. (2011b) prepared a superhydrophobic carbon nanotube (CNT) film by a simple spray-coating method without any further chemical modification. The surface wettability of the CNT film could be reversibly changed between superhydrophobic and superhydrophilic by alternating between a hot environment and ambient temperature due to the change of surface charges on the CNT film. Facile one-step spray-deposition process for the fabrication of superhydrophobic and superoleophilic SiO_2-NP (SiO_2-NPs were chemically modified with trimethylchlorosilane) films showing a quick temperature-responsive wettability transition was also reported by Zhang et al. (2012). When the as-prepared film was kept in a freezer until the surface temperature dropped down to −15 °C, it switched from superhydrophobic (water CA was about 168°) to hydrophilic (water CA was about 71°), and immediately returned to superhydrophobic by leaving the sample at room temperature for only 3 min. This process could be repeated several times, and good reversibility of the surface wettability was confirmed. This temperature-responsive transition was considered to be related to water vapor condensation on the surface.

1.4.4 Light Response

Several types of photo-sensitive materials have been used to prepare light-responsive smart surfaces and interfaces. Inorganic oxides, such as TiO_2 (Feng et al. 2005; Zhang et al. 2007; Sun et al. 2001), ZnO (Sun et al. 2001; Feng et al. 2004), SnO_2 (Zhu et al. 2006), WO_3 (Wang et al. 2006), and so on are well known to show reversibly switchable wettability.

Among them, TiO_2 particles have been widely used to prepare light-sensitive smart surfaces and interfaces. The main role of the particulate morphology is to provide surface roughness and so increase CAs (Gondal et al. 2014). Whereas the choice of particle material (TiO_2) gives photocatalytic decomposition of organic contaminants. Wang et al. (2016b) prepared a smart surface consisting of TiO_2-NPs doped polyvinylidene fluoride (PVDF) nanofibers by electrospinning, which formed beads-on-string structures with hierarchical roughness. These nanofiber membranes where used in separation of oil/water mixtures and showed switching behavior when UV (or sunlight) irradiated (water CA of 0°) or heat treated (water CA of ~152°) by selectively allowing water or oil to pass, respectively. In addition, these nanofiber membranes exhibited anti-fouling and self-cleaning properties because of the photocatalytic property of TiO_2, as shown in Fig. 1.14. Such properties may enable their reusability for practical applications.

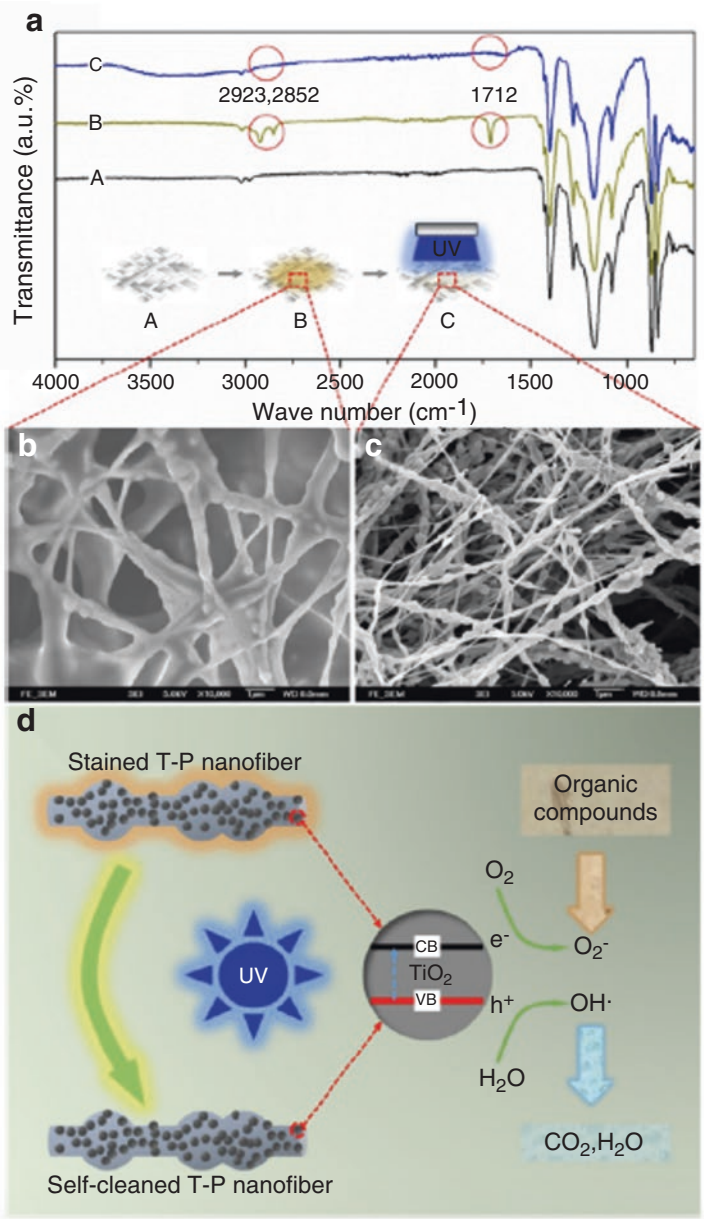

Fig. 1.14 Anti-fouling and self-cleaning behavior of the TiO_2-PVDF nanofibrous membrane. (**a**) FTIR spectrum showing the chemical component difference among the TiO_2-PVDF membrane before and after being stained by oleic acid and the stained TiO_2-PVDF membrane treated by UV-irradiation. FE-SEM images show the top surface of the stained TiO_2-PVDF membrane before (**b**) and after (**c**) UV-irradiation. (**d**) Illustration of the self-cleaning behavior of the TiO_2-PVDF nanofibers and the photocatalytic mechanism of TiO_2-NPs. (Reproduced with permission from (Wang et al. 2016b), Copyright 2016 The American Chemical Society)

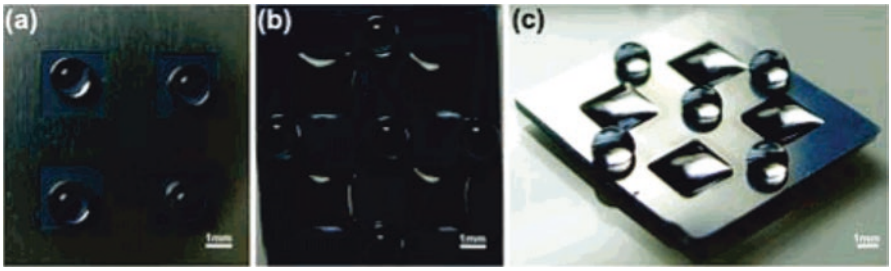

Fig. 1.15 Photographs of substrates with patterned extreme wetting properties. (**a**) Photomask and water droplet profiles on the as-prepared substrate. (**b**) Top and (**c**) angled views of water droplet profiles on the patterned substrate as a result of site-selective UV irradiation. (Reproduced with permission from (Lim et al. 2006), Copyright 2006 The American Chemical Society)

Besides inorganic oxides, some organic materials containing photochromic functional groups (azobenzene (Delorme et al. 2005), spiropyran (Rosario et al. 2002), dipyridylethylene (Cooper et al. 2004), and stilbene (Driscoll et al. 2007)) have an ability to change a reversible conformation through UV/visible irradiation, resulting in changes in their wetting properties. Among these photo-sensitive materials, azobenzene and its derivatives are particularly promising.

For example, Lim et al. (2006) first reported superhydrophobic and superhydrophilic transitions of organic molecules under UV/visible irradiation. Using 7-[(trifluoromethoxyphenylazo) phenoxy]pentanoic acid (CF_3AZO, photo switchable agent), they prepared organic-inorganic hybrid multilayer films by LBL deposition using poly(allylamine hydrochloride) (PAH) and SiO_2-NPs as the polycation and polyanion, respectively. With increases in the number of PAH/SiO_2-NPs bilayers ((PAH/SiO_2-NPs)$_n$), the water CA gradually increased from 76° (flat, $n = 0$) to 152° ($n = 9$) in the absence of UV light (*trans* isomer). When the samples were irradiated with UV light (*cis* isomer), the water CA slowly decreased from 71° (flat, $n = 0$) to 5° ($n = 9$). In this fashion, the surfaces showed reversible switching between superhydrophobicity and superhydrophilicity upon alternating between UV and visible light irradiation. They have also successfully prepared erasable and rewritable micropatterns of extreme wetting properties based on a site-selective UV irradiation (Fig. 1.15).

Although these photo-sensitive organic materials are particularly promising because of their easy chemical modification and reaction diversity, their photo, thermal, and chemical stabilities are inferior, compared to inorganic materials.

1.4.5 Electric Response

Changes in surface wettability of electro-responsive surfaces and interfaces are driven by the re-arrangement of charges and dipoles when an electric potential is applied between a liquid and a solid, resulting in a reduction in the interfacial energy

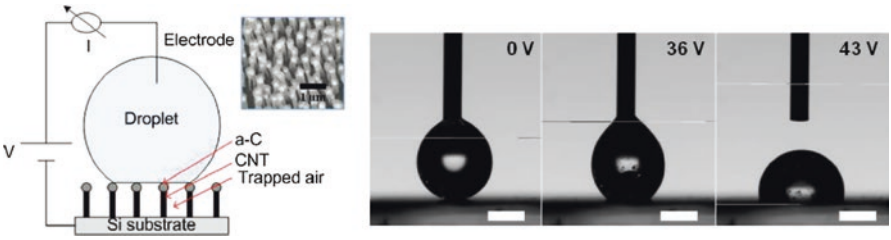

Fig. 1.16 The schematic diagram for electrowetting setup (left). The droplet is in contact with the a-C-NPs and air is trapped between neighboring CNTs in the Cassie state. The inset shows the microstructure of a-C/CNT nanocomposites. The electrowetting images for water at different potentials. The scale bar is 1 mm for all images (right). (Reproduced with permission from (Han et al. 2009), Copyright 2009 The American Chemical Society)

(increase in surface wettability). The advantages of using electrical potentials are the ability to control surface wettability without any changes in the surface composition and morphology. Thus, it is considered a simple, versatile, and effective external stimulus to switch surface wetting behavior (Xu et al. 2014; Mugele and Baret 2005; Kakade et al. 2008; Bodre and Pauporte 2009; Krupenkin et al. 2007; Han et al. 2009).

For instance, Krupenkin et al. (2007) successfully demonstrated fully reversible switching between the superhydrophobic Cassie-Baxter state and the hydrophilic Wenzel state on nanostructured surfaces by the application of an electrical voltage and current. Without an applied voltage, a water droplet on the nanograss substrate was unstable and highly mobile. When 35 V was applied, the water droplet underwent a sharp transition to the immobile state. After a short pulse of electrical current was transmitted through the nanograss substrate, the droplet returned to the original unstable state. Han et al. (2009) also reported an effective control of surface wettability of a nanostructured surface consisting of arrays of amorphous carbon (a-C)-NPs capped on CNTs using an electrowetting technique (Fig. 1.16 **left**). By applying a potential from 0 to 36 V between the water droplet and the solid surface, water CAs slowly reduced from 160° to 142°. When the CAs approached the threshold value (-142°), a transition from the "slippy" Cassie state to the "sticky" Wenzel state (final water CA was 104° at 43 V) was observed (Fig. 1.16 **right**).

1.4.6 Magnetic Response

Smart surfaces and interfaces which can respond to magnetic fields have been reported by Grigoryev et al. (2012) and Cheng et al. (2012c). As shown in Fig. 1.17, Grigoryev et al. (2012) fabricated Ni-wire arrays (micronails) with a high aspect ratio whose top was capped with μm-scale (between 4 and 8 μm) hemispherical

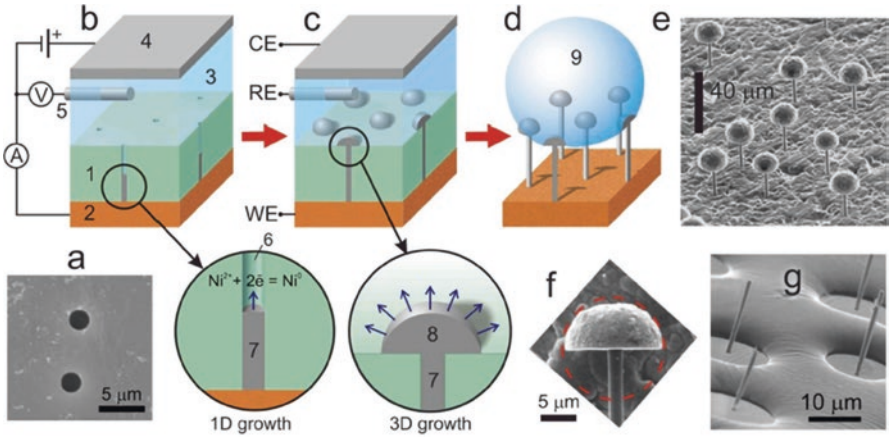

Fig. 1.17 Fabrication and characterization of Ni-micronails. (**a**) SEM micrograph of a PC template. (**b**) Three-electrode electrodeposition setup consisting of a track-etch template (*1*), a metal working electrode (WE) deposited on one side of the PC template (*2*), a Ni-electroplating bath (*3*), a Ni-counter electrode (CE) (*4*), and a reference electrode (RE) (*5*), the enlarged schematic shows the pore-confined 1D growth of Ni inside of the template pore (6), formation of a Ni wire leg (*7*). (**c**) Ni wires reach the top of the PC template and continue to grow. The enlarged schematic shows the unrestricted 3D growth of Ni on the template surface, resulting in the formation of a hemispherical cap (*8*). (**d**) The structure of a bed of Ni micronails after removal of the PC template, and supports the Cassie-Baxter regime (*9*). (**e**) SEM image of a cluster of electrodeposited Ni-micronails. (**f**) Magnification of SEM image of a single Ni-micronail. (**g**) SEM image showing the Cassie-Baxter state for an epoxy resin droplet sitting on a bed of Ni-micronails. The Ni-micronails were separated from the metal substrate to visualize the reverse side of the droplet. (Reproduced with permission from (Grigoryev et al. 2012), Copyright 2012 The American Chemical Society)

caps based on an area-selective electrodeposition using a polycarbonate (PC) membrane possessing uniform cylindrical pores. They demonstrated a wettability transition from superomniphobicity to omniphilicity by applying an external magnetic field. Ni-micronail surface covered with a self-assembled monolayer (SAM) of 1*H*,1*H*,2*H*,2*H*-perfluorodecanethiol showed superomniphobicity without a magnetic field, however, when an external magnetic field (50 mT) was applied and Ni-micronails were bent with an angle of 23° with the surface normal, the transition from the anti-wetting Cassie-Baxter state (water CA was 159° and *n*-hexadecane CA was 153°) to the wetting Wenzel state was observed. Cheng et al. (2012c) also demonstrated reversible wetting/dewetting transitions of microdroplets containing superparamagnetic Fe_3O_4-nanoparticles (NPs) on a highly hydrophobic microstructured Si surface. They successfully controlled the switching between the Cassie state (water CA of 145°) and the Wenzel state (water CA of 135°) by the intensity of the magnetic field and the concentration of Fe_3O_4-NPs in the microdroplet (Fig. 1.18).

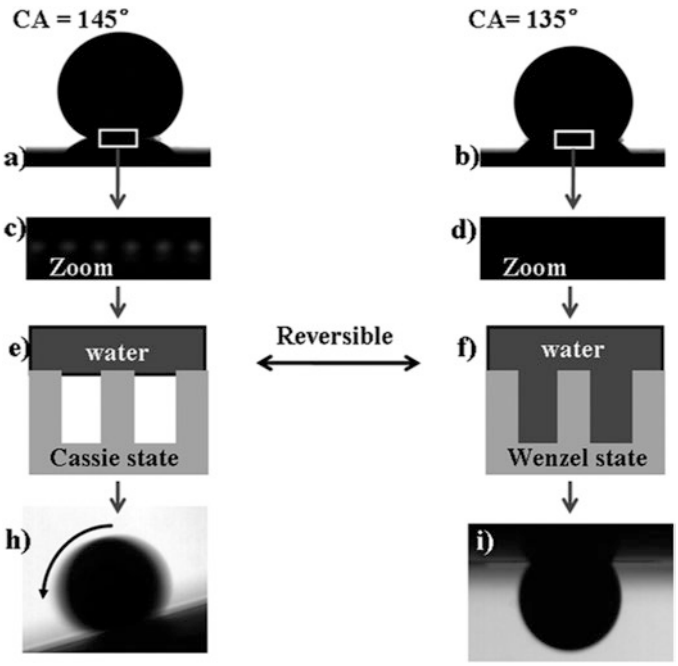

Fig. 1.18 Reversible transition between the Cassie state and the Wenzel state by application of the magnetic fields. (**a** and **b**) The superparamagnetic microdroplet resides in the Cassie state (CA of 145°) and the Wenzel state (CA of 135°), respectively. (**c** and **d**) Higher magnification photos of the interface between the liquid and the substrate with and without air, respectively. (**e** and **f**) Schematic illustration of the two wetting states. (**h** and **i**) In the Cassie state, a microdroplet can roll across the surface, while in the Wenzel state, it is pinned to the surface. (Reproduced with permission from (Cheng et al. 2012c), Copyright 2012 The American Chemical Society)

1.4.7 Gas Response

Zhu et al. reported ammonia-gas responsive surfaces showing switchable wettability on micro/nanostructured indium hydroxide ($In(OH)_3$) films (Zhu et al. 2008) and polyaniline-coated fabrics (Zhu et al. 2007). In the former case, the films were superhydrophobic in air with a water CA of 150.4°, while their surfaces turned to superhydrophilic with a water CA of 0° after exposure to an ammonia vapor. Li et al. (2014b) reported CO_2-gas responsive surface covered with a SAM of *N*-(2-aminoethyl)-5-(1,2-dithiolan-3-yl) pentanamide amidine (NADPA) on Au substrates *via* molecular self-assembly technique. The surface wettability of the NADPA-SAM showed reversible switching because of reversion of the amidine conjugation systems, which was caused by reversible protonation/deprotonation in the presence/absence of CO_2 gas (Fig. 1.19).

Che et al. (2015) also reported CO_2-gas responsive nanofibrous membranes (average diameter of about 700 nm), which are capable of oil/water separation applications. They prepared polymeric membranes using poly(methyl methacrylate)-

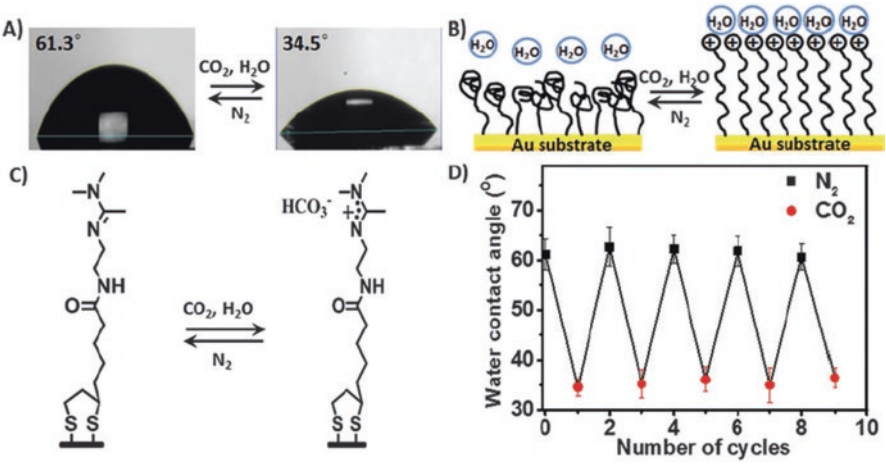

Fig. 1.19 CO_2-responsive switching of the NADPA-SAM. (**a**) A photographic image of the water droplet on a NADPA modified surface before (left) and after (right) the stimuli of CO_2. (**b**) A schematic diagram stimuli-induced transition of surface wettability. (**c**) Changes in the chemical structure of amidine. (**d**) Reversible switching of water CAs. (Reproduced with permission from (Li et al. 2014b), Copyright 2014 The Royal Society of Chemistry)

co-poly(*N,N*-diethylaminoethyl methacrylate) (PMMA-*co*-PDEAEMA) by electrospinning, and then tested for water and oil wettability. They successfully demonstrated selective switching for an oil/water separation system using CO_2 or N_2 gas flow. As shown in Fig. 1.20, when an oil/water mixture was introduced to the membrane, oil could pass easily, while water remained on the membrane surface because the membrane surface showed hydrophobic and oleophilic properties. In contrast, when the membranes were submerged in water with CO_2 gas bubbling through the liquid for a few minutes, the separation results dramatically changed. In that case, water could be separated and oil remained on the membrane surface.

1.4.8 Solvent Response

Solvent-responsive smart surfaces and interfaces are influenced by the surrounding media, and their switchable wettability is governed by change in interfacial free energy, which is driven by conversion or rearrangement of polymer chains, induced by solvents (Minko et al. 2003; Motornov et al. 2003; Liu et al. 2005; Song et al. 2007; Wang et al. 2009).

Minko et al. (2003) reported the control of surface wettability by exposing the polymer films to different solvents (toluene, 1,4-dioxane and acidic water). They attached polymer chains of PSF-COOH (PSF: pentafluorostyrene) and PVP-COOH (PVP: poly(*N*-vinylpyrrolidone)) to flat and plasma-etched needle-like PTFE sub-

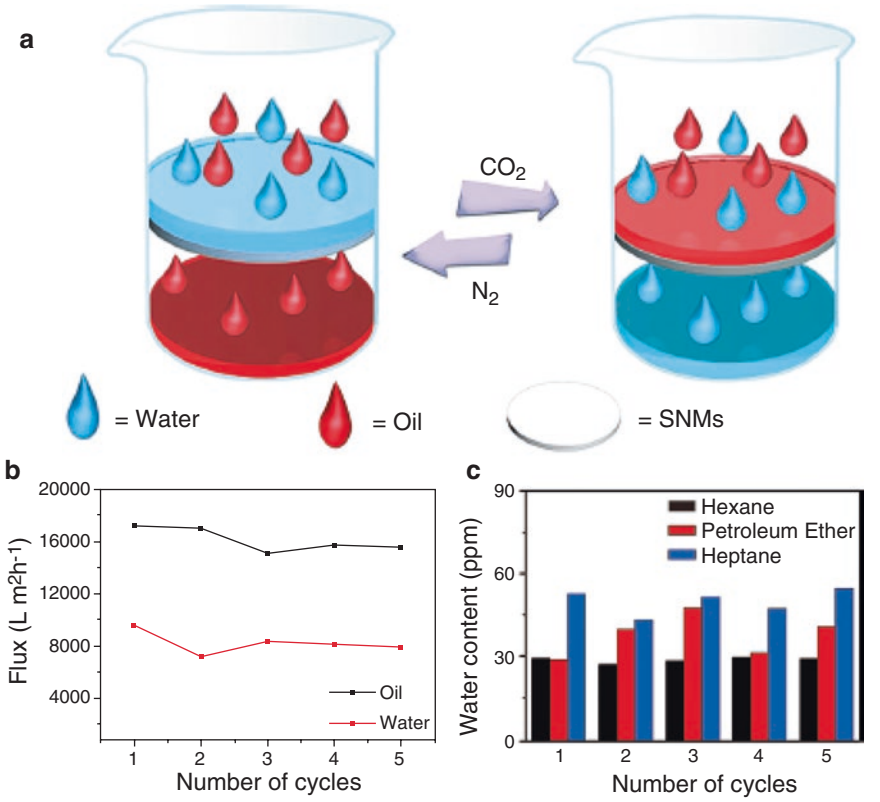

Fig. 1.20 (**a**) Representation of the CO_2 switchable oil/water on-off switch. (**b**) Variations in the flux of oil and water in the absence and presence of CO_2, respectively. (**c**) Water content in oil in the filtrate after permeating oil/water mixtures through the smart nanostructured membranes. (Reproduced with permission from (Che et al. 2015), Copyright 2015 Wiley-VCH Verlag GmbH & Co. KGaA, Weinheim)

strates terminated with hydroxyl and amino groups, which were introduced by the plasma treatment. In the case of selective solvents, upon exposure to toluene, the top of the film surface was predominantly occupied by the PSF component, while upon exposure to acidic water (pH 3), the PSF formed round domains and was buried in the PVP matrix. On the other hand, in the case of non-selective solvents, both polymer components were present on the surface (Fig. 1.21). As a result, after exposure to toluene, acidic water (pH 3), and 1,4-dioxane, the advancing CA (θ_A) of water on the flat substrate was measured to be 118°, 25°, and 75°, respectively. This switching behavior was amplified by the surface roughness. After exposure to toluene, the θ_A of water was increased to 160° and a water droplet rolled easily on the surface, showing low CA hysteresis.

Wang et al. (2009) reported an unusual solvent-responsive smart surface prepared from double amino acid (aspartic acid (AA) and cysteine (Cy)) units grafted

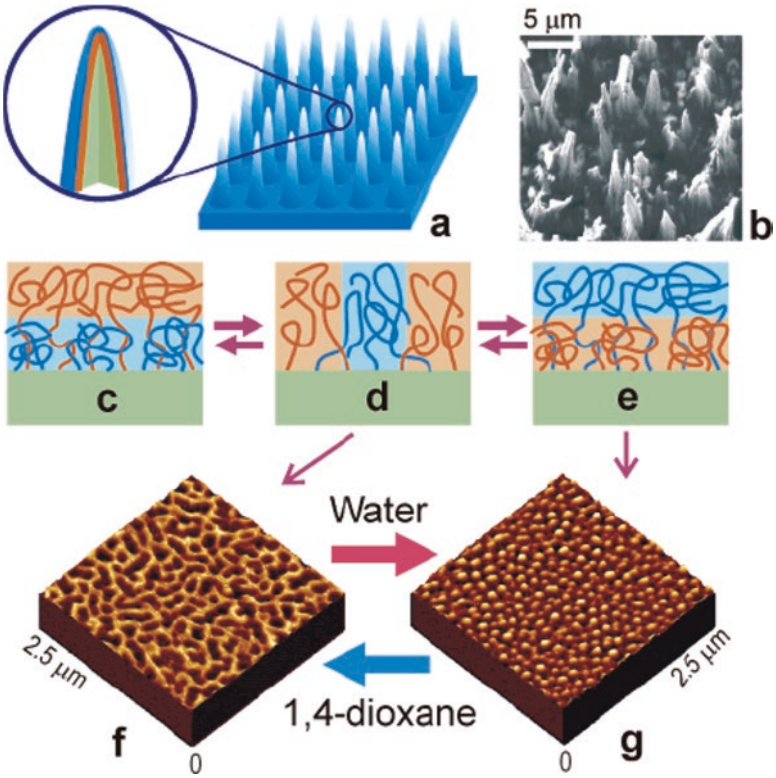

Fig. 1.21 Two-level structure of self-adaptive surfaces (SAS). (**a**) Schematic representation of needle-like surface morphology of the PTFE surface (first level). (**b**) SEM image of the PTFE film after 600 s of plasma etching. (**c**–**e**) Each needle is covered by a covalently grafted mixed brush that consists of hydrophobic and hydrophilic polymers (second level). Its morphology results from an interplay between lateral and vertical phase segregation of the polymers, which switches the morphology and surface properties upon exposure to different solvents. (**c** and **e**) In selective solvents, the preferred polymer preferentially occupies the top of the surface. (**d**) In non-selective solvents, both polymers are present in the top layer. (**f** and **g**) AFM images (model smooth substrate) of the different morphologies after exposure to different solvents. (Reproduced with permission from (Minko et al. 2003), Copyright 2003 The American Chemical Society)

PNiPAAm copolymer film (PNiPAAm-*co*-Cy&AA)). The changes in water CA in response to the solvents (water and methanol) on a flat Si substrate were only 11° (water CAs after water and methanol treatments were about 86° and 75°, respectively). When a structured Si substrate consisting of well-aligned square micro-pillars (side length of about 10 μm and separation of about 12 μm) with nano-fibrous structures on the top of each pillar was used, water treatment induced a dramatic increase of hydrophobicity, changing from slightly hydrophilic (water CA of about 72°) to superhydrophobic (water CA was about 156°). However, the reversibility of the wettability switching again was poor. The authors then replaced pure methanol with the mixture of methanol and alkali. They confirmed the

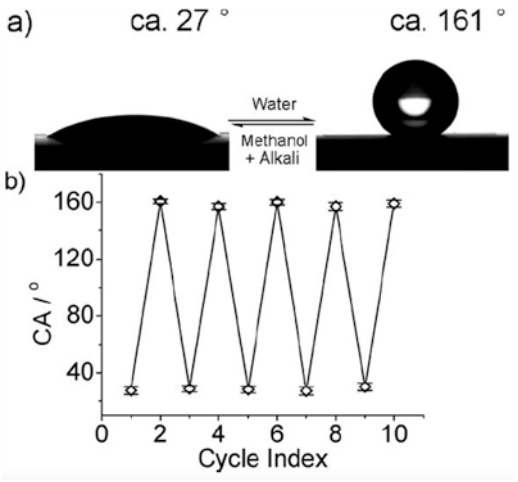

Fig. 1.22 Reversible wettability switching between high hydrophilicity and superhydrophobicity for a PNiPAAm-co-Cy&AA film on a structured substrate when treated with water and methanol-alkali solution alternately: (**a**) water drop profiles, (**b**) cycling experiment. (Reproduced with permission from (Wang et al. 2009), Copyright 2009 The Royal Society of Chemistry)

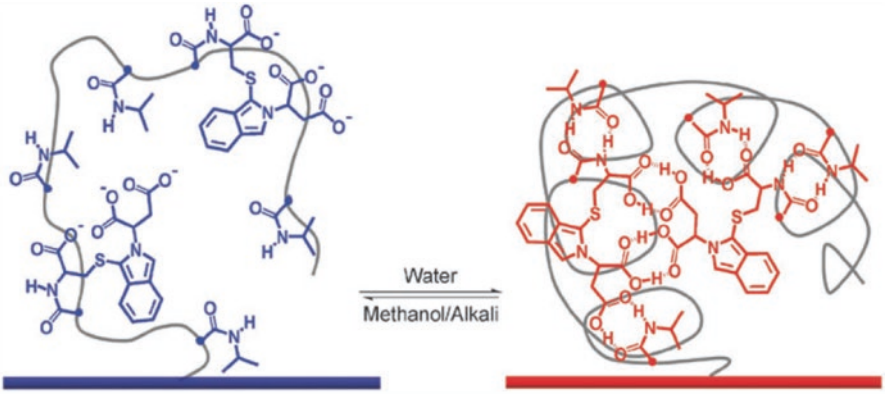

Fig. 1.23 Schematic diagram for the possible mechanism of the solvent-responsive wettability on PNiPAAm-*co*-Cy&AA copolymer film. In this mechanism, methanol-alkali or water treatments influence both the formation or cleavage of the intramolecular hydrogen-bonding, and the aggregation or dispersion of the anions inside the polymer film, which results in a change of the loose or wound conformations of polymer, and the wettability change of the film. (Reproduced with permission from (Wang et al. 2009), Copyright 2009 The Royal Society of Chemistry)

remarkable changes in water CA (water CAs after water and methanol-alkali treatments were about 161° and 27°, respectively) and good reversibility (Fig. 1.22). The methanol treatment weakens both the hydrophobic and hydrogen bonding interactions, and addition of alkali, leads to highly charged carboxyl groups and a highly hydrophilic surface (Fig. 1.23, **left**). In contrast, once the polymer surface contacted water, due to the solvophobic effect and the dielectric properties of water media, the polymer switched back to the bound state, leading to the hydrophobic surface (Fig. 1.23, **right**).

1.5 Summary

This chapter briefly summarizes the basic theories of surface wetting/dewetting properties of flat and rough solid surfaces, such as static/dynamic contact angles (CAs), CA hysteresis, Young's, Wenzel's, and Cassie-Baxter's equations. Although static CA (θ_S) measurements are a conventional way to characterize the surface properties and understand liquid-solid interactions, it has been recently recognized that static dewetting properties of solid surfaces (conventional θ_S values) alone do not closely reflect actual wetting/dewetting properties. Thus, instead of relying on the magnitude of θ_S values, the measurement of dynamic wettability, including the advancing (θ_A) and receding (θ_R) CAs, CA hysteresis, and tilt angles (θ_T) are required to accurately characterize the wetting/dewetting properties of a solid surface. Therefore, besides θ_S values, these factors are now taken into account in the latest definition of super-liquid-repellent (SLR) surfaces and interfaces.

This chapter also introduced an overview of the typical examples of smart surfaces and interfaces possessing controllable wetting/dewetting properties by different external stimuli, such as pH, temperature, light, solvent, mechanical stress, and electric/magnetic fields and so on. In this chapter, we focused on the surfaces/interfaces showing a response to only one of the external stimuli mentioned above. However, such simple responses of the functional surfaces limit their practical applications under complicated conditions. Thus, further development of dual and multiple responsive smart surfaces/interfaces is also necessary. Although these stimuli-responsive surfaces/interfaces, which take advantage of the SLR properties are promising, they are in their infancy and still very challenging. We hope that this book will enhance interest for researchers and engineers in this new research field.

References

Agarwal S, Greiner A, Wendorff JH (2013) Functional materials by electrospinning of polymers. Prog Polym Sci 38:963–991

Alayande SO, Dare EO, Msagati TAM, Akinlabi AK, Aiyedun PO (2016) Superhydrophobic and superoleophillic surface of porous beaded electrospun polystrene and polysytrene-zeolite fiber for crude oil-water separation. Phys Chem Earth 92:7–13

Arslan O, Aytac Z, Uyar T (2016) Superhydrophobic, hybrid, electrospun cellulose acetate nanofibrous mats for oil/water separation by tailored surface modification. ACS Appl Mater Interfaces 8:19747–19754

Barbey R, Lavanant L, Paripovic D, Schüwer N, Sugnaux C, Tugulu S, Klok HA (2009) Polymer brushes via surface-initiated controlled radical polymerization: synthesis, characterization, properties, and applications. Chem Rev 109:5437–5527

Bhardwaj N, Kundu SC (2010) Electrospinning: a fascinating fiber fabrication technique. Biotechnol Adv 28:325–347

Bhushan B, Jung YC (2011) Natural and biomimetic artificial surfaces for superhydrophobicity, self-cleaning, low adhesion, and drag reduction. Prog Mater Sci 56:1–108

Bodre C, Pauporte T (2009) Nanostructured ZnO-based surface with reversible electrochemically adjustable wettability. Adv Mater 21:697–701

Brown PS, Bhushan B (2016) Durable, superoleophobic polymer–nanoparticle composite surfaces with re-entrant geometry via solvent-induced phase transformation. Sci Rep 6:21048

Byun J, Shin J, Kwon S, Jang S, Kim JK (2012) Fast and reversibly switchable wettability induced by a photothermal effect. Chem Commun 48:9278–9280

Cassie ABD, Baxter S (1944) Wettability of porous surfaces. Trans Faraday Soc 40:546–551

Che H, Huo M, Peng L, Fang T, Liu N, Feng L, Wei Y, Yuan J (2015) Co2-responsive nanofibrous membranes with switchable oil/water wettability. Angew Chem Int Ed 54:8934–8938

Chen W, Fadeev AY, Hsieh MC, Öner D, Youngblood J, McCarthy TJ (1999) Ultrahydrophobic and ultralyophobic surfaces: some comments and examples. Langmuir 15:3395–3399

Chen L, Liu MJ, Lin L, Zhang T, Ma J, Song YL, Jiang L (2010) Thermal-responsive hydrogel surface: tunable wettability and adhesion to oil at the water/solid interface. Soft Matter 6:2708–2712

Cheng DF, Urata C, Yagihashi M, Hozumi A (2012a) A statically oleophilic but dynamically oleophobic smooth nonperfluorinated surface. Angew Chem Int Ed 51:2956–2959

Cheng DF, Urata C, Masheder B, Hozumi A (2012b) A physical approach to specifically improve the mobility of alkane liquid drops. J Am Chem Soc 134:10191–10199

Cheng Z, Lai H, Zhang NQ, Sun KN, Jiang L (2012c) Magnetically induced reversible transition between cassie and wenzel states of superparamagnetic microdroplets on highly hydrophobic silicon surface. J Phys Chem C 116:18796–18802

Chung JY, Youngblood JP, Stafford CM (2007) Anisotropic wetting on tunable micro-wrinkled surface. Soft Matter 3:1163–1169

Cooper CGF, MacDonald JC, Soto E, McGimpsey WG (2004) Non-covalent assembly of a photoswitchable surface. J Am Chem Soc 126:1032–1033

Crevoisier GD, Fabre P, Corpart JM, Leibler L (1999) Switchable tackiness and wettability of a liquid crystalline polymer. Science 285:1246–1249

Decher G (1997) Fuzzy nanoassemblies: toward layered polymeric multicomposites. Science 277:1232–1237

Delorme N, Bardeau JF, Bulou A, Poncin-Epaillard F (2005) Azobenzene-containing monolayer with photoswitchable wettability. Langmuir 21:12278–12282

Deng X, Mammen L, Butt HJ, Vollmer D (2012) Candle soot as a template for a transparent robust superamphiphobic coating. Science 335:67–70

Ding B, Wang M, Wang X, Yu J, Sun G (2010) Electrospun nanomaterials for ultrasensitive sensors. Mater Today 13:16–27

Doshi J, Reneker DH (1995) Electrospinning process and applications of electrospun fibers. J Electrost 35:151–160

Driscoll PF, Purohit N, Wanichacheva N, Lambert CR, McGimpsey WG (2007) Reversible photoswitchable wettability in noncovalently assembled multilayered films. Langmuir 23:13181–13187

Dunderdale GJ, Urata C, Miranda DF, Hozumi A (2014) Large-scale and environmentally friendly synthesis of pH-responsive oil-repellent polymer brush surfaces under ambient conditions. ACS Appl Mater Interfaces 6:11864–11868

Dunderdale GJ, Urata C, Sato T, England MW, Hozumi A (2015) Continuous, high-speed, and efficient oil/water separation using meshes with antagonistic wetting properties. ACS Appl Mater Interfaces 7:18915–18919

Fang W, Liu L, Li T, Dang Z, Qiao C, Xu J, Wang Y (2016) Electrospun N-substituted polyurethane membranes with self-healing ability for self-cleaning and oil/water separation. Chem-Eur J 22:878–883

Feng X, Jiang L (2006) Design and creation of superwetting/antiwetting surfaces. Adv Mater 18:3063–3078

Feng C, Zhang Y, Jin J, Song Y, Xie L, Qu G, Jiang L, Zhu D (2001) Reversible wettability of photoresponsive fluorine-containing azobenzene polymer in Langmuir-Blodgett films. Langmuir 17:4593–4597

Feng XJ, Feng L, Jin MH, Zhai J, Jiang L, Zhu DB (2004) Reversible super-hydrophobicity to super-hydrophilicity transition of aligned ZnO nanorod films. J Am Chem Soc 126:62–63

Feng XJ, Zhai J, Jiang L (2005) The fabrication and switchable superhydrophobicity of TiO_2 nanorod films. Angew Chem Int Ed 44:5115–5118

Forsberg PSH, Priest C, Brinkmann M, Sedev R, Ralston J (2010) Contact line pinning on microstructured surfaces for liquids in the Wenzel state. Langmuir 26:860–865

Fu Q, Rao GVR, Basame SB, Keller DJ, Artyushkova K, Fulghum JE, López GP (2004) Reversible control of free energy and topography of nanostructured surfaces. J Am Chem Soc 126:8904–8905

Furmidge CGL (1962) Studies at phase interfaces. I. The sliding of liquid drops on solid surfaces and a theory for spray retention. J Colloid Sci 17:309–324

Gao L, McCarthy TJ (2006a) The "lotus effect" explained: two reasons why two length scales of topography are important. Langmuir 22:2966–2967

Gao L, McCarthy TJ (2006b) Contact angle hysteresis explained. Langmuir 22:6234–6237

Gao L, McCarthy TJ (2009) Wetting 101°. Langmuir 25:14105–14115

Gondal MA, Sadullah MS, Dastageer MA, McKinley GH, Panchanathan D, Varanasi KK (2014) Study of factors governing oil-water separation process using TiO_2 films prepared by spray deposition of nanoparticle dispersions. ACS Appl Mater Interfaces 6:13422–13429

Grigoryev A, Tokarev I, Kornev KG, Luzinov I, Minko S (2012) Superomniphobic magnetic microtextures with remote wetting control. J Am Chem Soc 134:12916–12919

Guo F, Guo Z (2016) Inspired smart materials with external stimuli responsive wettability: a review. RSC Adv 6:36623–36641

Han ZJ, Tay B, Tan C, Shakerzadeh M, Ostrikov K (2009) Electrowetting control of cassie-to-wenzel transitions in superhydrophobic carbon nanotube-based nanocomposites. ACS Nano 3:3031–3036

Hozumi A, Takai O (1997) Preparation of ultra water-repellent films by microwave plasma-enhanced CVD. Thin Solid Film 303:222–225

Huang ZM, Zhang YZ, Kotaki M, Ramakrishna S (2003) Compos Sci Technol 63:2223–2253

Huang M, Si Y, Tang X, Zhu Z, Ding B, Liu L, Zheng G, Luo W, Yu J (2013) Gravity driven separation of emulsified oil-water mixtures utilizing *in situ* polymerized superhydrophobic and superoleophilic nanofibrous membranes. J Mater Chem A 1:14071–14074

Huang X, Sun YJ, Soh S (2015) Stimuli-responsive surfaces for tunable and reversible control of wettability. Adv Mater 27:4062–4068

Huber DL, Manginell RP, Samara MA, Kim BI, Bunker BC (2003) Programmed adsorption and release of proteins in a microfluidic device. Science 301:352–354

Jain P, Baker GL, Bruening ML (2009) Applications of polymer brushes in protein analysis and purification. Annu Rev Anal Chem 2:387–408

Jin M, Feng X, Feng L, Sun T, Zhai J, Li T, Jiang L (2005) Superhydrophobic aligned polystyrene nanotube films with high adhesive force. Adv Mater 17:1977–1981

Jin CF, Yan RS, Huang JG (2011) Cellulose substance with reversible photo-responsive wettability by surface modification. J Mater Chem 21:17519–17525

Jones DM, Huck WTS (2001) Controlled surface-initiated polymerizations in aqueous media. Adv Mater 13:1256–1259

Kakade B, Mehta R, Durge A, Kulkarni S, Pillai V (2008) Electric field induced, superhydrophobic to superhydrophilic switching in multiwalled carbon nanotube papers. Nano Lett 8:2693–2696

Kawasaki K (1960) Study of wettability of polymers by sliding of water drop. J Colloid Sci 15:402–407

Kim YJ, Ebara M, Aoyagi T (2012) A smart nanofiber web that captures and releases cells. Angew Chem Int Ed 51:10537–10541

Kim YJ, Ebara M, Aoyagi T (2013) A smart hyperthermia nanofiber with switchable drug release for inducing cancer apoptosis. Adv Funct Mater 23:5753–5761

Koenig M, Magerl D, Philipp M, Eichhorn KJ, Müller M, Müller Buschaum P, Stamm M, Uhlmann P (2014) Nanocomposite coatings with stimuli-responsive catalytic activity. RSC Adv 4:17579–17586

Kota AK, Kwon G, Choi W, Mabry JM, Tuteja A (2012) Hygro-responsive membranes for effective oil-water separation. Nat Commun 3:1025

Kota AK, Kwon G, Tuteja A (2014) The design and applications of superomniphobic surfaces. NPG Asia Mater 6:e109

Krupenkin TN, Taylor JA, Wang EN, Kolodner P, Hodes M, Salamon TR (2007) Reversible wetting-dewetting transitions on electrically tunable superhydrophobic nanostructured surfaces. Langmuir 23:9128–9133

Lafuma A, Qéré D (2003) Superhydrophobic states. Nat Mater 2:457–460

Lahann J, Mitragotri S, Tran TN, Kaido H, Sundaram J, Choi IS, Hoffer S, Somorjai GA, Langer R (2003) A reversibly switching surface. Science 299:371–374

Lee KH, Kim HY, Khil MS, Ra YM, Lee DR (2003) Characterization of nano-structured poly(ε-caprolactone) nonwoven mats via electrospinning. Polymer 44:1287–1294

Li D, Xia Y (2004) Electrospinning of nanofibers: reinventing the wheel? Adv Mater 16:1151–1170

Li C, Guo RW, Jiang X, Hu SX, Li L, Cao XY, Yang H, Song YL, Ma YM, Jiang L (2009) Reversible switching of water-droplet mobility on a superhydrophobic surface based on a phase transition of a side-chain liquid-crystal polymer. Adv Mater 21:4254–4258

Li X, Hu D, Huang K, Yang C (2014a) Hierarchical rough surfaces formed by LBL self-assembly for oil-water separation. J Mater Chem A 2:11830–11838

Li N, Thia L, Wang X (2014b) A CO_2-responsive surface with an amidine-terminated self-assembled monolayer for stimuli-induced selective adsorption. Chem Commun 50:4003–4006

Li JJ, Zhou YN, Jiang ZD, Luo ZH (2016a) Electrospun fibrous mat with pH-switchable superwettability that can separate layered oil/water mixtures. Langmuir 32:13358–13366

Li JJ, Zhu LT, Luo ZH (2016b) Electrospun fibrous mat with pH-switchable superwettability that can separate layered oil/water mixtures. Chem Eng J 287:474–481

Lim HS, Han JT, Kwak D, Jin M, Cho K (2006) Photoreversibly switchable superhydrophobic surface with erasable and rewritable pattern. J Am Chem Soc 128:14458–14459

Lin P, Yang S (2009) Mechanically switchable wetting on wrinkled elastomers with dual-scale roughness. Soft Matter 5:1011–1018

Liu CT, Liu YL (2016) pH-induced switches of the oil- and water-selectivity of crosslinked polymeric membranes for gravity-driven oil-water separation. J Mater Chem A 4:13543–13548

Liu Y, Mu L, Liu BH, Kong JL (2005) Controlled switchable surface. Chem-Eur J 11:2622–2631

Liu FM, Pang J, Wang CY, Wang LY (2013) Solvent-responsive wettability of self-assembled monolayers of dithiooctanoic acid derivatives bearing *N*,*N*-disubstituted amide groups. Langmuir 29:13003–13007

Liu H, Zhang X, Wang S, Jiang L (2015) Underwater thermoresponsive surface with switchable oil-wettability between superoleophobicity and superoleophilicity. Small 11:3338–3342

Lu YM, Sarshar MA, Du K, Chou T, Choi CH, Sukhishvili SA (2013) Large-amplitude, reversible, pH-triggered wetting transitions enabled by layer-by-layer films. ACS Appl Mater Interfaces 5:12617–12623

Ma W, Zhang Q, Hua D, Xiong R, Zhao J, Rao W, Huang S, Zhan X, Chen F, Huang C (2016a) Electrospun fibers for oil-water separation. RSC Adv 6:12868–12884

Ma W, Zhang Q, Samal SK, Wang F, Gao B, Pan H, Xu H, Yao J, Zhan X, De Smedt SC, Huang C (2016b) Core-sheath structured electrospun nanofibrous membranes for oil-water separation. RSC Adv 6:41861–41870

Marmur A (2003) Wetting on hydrophobic rough surfaces: to be heterogeneous or not to be? Langmuir 19:8343–8348

Matyjaszewski K, Tsarevsky N (2009) Nanostructured functional materials prepared by atom transfer radical polymerization. Nat Chem 1:276–288

Megelski S, Stephens JS, Bruce Chase D, Rabolt JF (2002) Micro- and nanostructured surface morphology on electrospun polymer fibers. Macromolecules 35:8456–8466

Minko S, Müller M, Motornov M, Nitschke M, Grundke K, Stamm M (2003) Two-level structured self-adaptive surfaces with reversibly tunable properties. J Am Chem Soc 125:3896–3900

Misra M, Singh N, Gupta RK (2017) Enhanced visible-light-driven photocatalytic activity of Au@Ag core-shell bimetallic nanoparticles immobilized on electrospun TiO_2 nanofibers for degradation of organic compounds. Cat Sci Technol 7:570–580

Motornov M, Minko S, Eichhorn KJ, Nitschke M, Simon F, Stamm M (2003) Reversible tuning of wetting behavior of polymer surface with responsive polymer brushes. Langmuir 19:8077–8085

Mugele F, Baret JC (2005) Electrowetting: from basics to applications. J Phys Condens Matter 17:705–774

Ning LQ, Xu NK, Wang R, Liu Y (2015) Fibrous membranes electrospun from the suspension polymerization product of styrene and butyl acrylate for oil-water separation. RSC Adv 5:57101–57113

Nosonovsky M (2007) Multiscale roughness and stability of superhydrophobic biomimetic interfaces. Langmuir 23:3157–3161

Obaid M, Tolba GMK, Motlak M, Fadali OA, Khalil KA, Almajid AA, Kim B, Barakat NAM (2015a) Effective polysulfone-amorphous SiO_2 NPs electrospun nanofiber membrane for high flux oil/water separation. Chem Eng J 279:631–638

Obaid M, Barakat NAM, Fadali OA, Al-Meer S, Elsaid K, Khalil KA (2015b) Stable and effective super-hydrophilic polysulfone nanofiber mats for oil/water separation. Polymer 72:125–133

Onda T, Shibuichi S, Satoh N, Tsujii K (1996) Super-water-repellent fractal surfaces. Langmuir 12:2125–2127

Pan S, Kota AK, Mabry JM, Tuteja A (2013) Superomniphobic surfaces for effective chemical shielding. J Am Chem Soc 135:578–581

Qiu Y, Park K (2001) Environment-sensitive hydrogels for drug delivery. Adv Drug Deliv Rev 53:321–339

Ramakrishna S, Fujihara K, Teo WE, Yong T, Ma Z, Ramaseshan R (2006) Electrospun nanofibers: solving global issues. Mater Today 9:40–50

Rosario R, Gust D, Hayes M, Jahnke F, Springer J, Garcia AA (2002) Photon-modulated wettability changes on spiropyran-coated surfaces. Langmuir 18:8062–8069

Sarbatly R, Krishnaiah D, Kamin Z (2016) A review of polymer nanofibres by electrospinning and their application in oil-water separation for cleaning up marine oil spills. Mar Pollut Bull 106:8–16

Simakova A, Averick SE, Konkolewicz D, Matyjaszewski K (2012) Aqueous ARGET ATRP. Macromolecules 45:6371–6379

Singh N, Mondal K, Misra M, Sharma A, Gupta RK (2016) Quantum dot sensitized electrospun mesoporous titanium dioxide hollow nanofibers for photocatalytic applications. RSC Adv 6:48109–48119

Song XY, Cao MW, Han YC, Wang YL, Kwak JCT (2007) Adsorption of hydrophobically modified poly(acrylamide)-*co*-(acrylic acid) on an amino-functionalized surface and its response to the external solvent environment. Langmuir 23:4279–4285

Sun TL, Qing GY (2011) Biomimetic smart interface materials for biological applications. Adv Mater 23:H57–H77

Sun RD, Nakajima A, Fujishima A, Watanabe T, Hashimoto K (2001) Photoinduced surface wettability conversion of ZnO and TiO_2 thin films. J Phys Chem B 105:1984–1990

Sun T, Wang G, Feng L, Liu B, Ma Y, Jiang L, Zhu D (2004) Reversible switching between superhydrophilicity and superhydrophobicity. Angew Chem Int Ed 43:357–360

Tai MH, Gao P, Tan BYL, Sun DD, Leckie JO (2014) Highly efficient and flexible electrospun carbon-silica nanofibrous membrane for ultrafast gravity-driven oil-water separation. ACS Appl Mater Interfaces 6:9393–9401

Tian Y, Su B, Jiang L (2014) Interfacial material system exhibiting superwettability. Adv Mater 26:6872–6897

Tsujii K, Yamamoto T, Onda T, Shibuichi S (1997) Super oil-repellent surfaces. Angew Chem Int Ed Engl 36:1011–1012

Tuteja A, Choi W, Ma ML, Mabry JM, Mazzella SA, Rutledge GC, McKinley GH, Cohen RE (2007) Designing superoleophobic surfaces. Science 318:1618–1622

Verho T, Bower C, Andrew P, Franssila S, Ikkala O, Ras RHA (2011) Mechanically durable superhydrophobic surface. Adv Mater 23:673–678

Wang Y, Bhushan B (2015) Wear-resistant and antismudge superoleophobic coating on polyethylene terephthalate substrate using SiO_2 nanoparticles. ACS Appl Matter Interface 7:743–755

Wang B, Guo ZG (2013) pH-responsive bidirectional oil-water separation material. Chem Commun 49:9416–9418

Wang GY, Zhang TY (2012) Easy route to the wettability cycling of copper surface between superhydrophobicity and superhydrophilicity. ACS Appl Mater Interfaces 4:273–279

Wang S, Feng X, Yao J, Jiang L (2006) Controlling wettability and photochromism in a dual-responsive tungsten oxide film. Angew Chem Int Ed 45:1264–1267

Wang X, Qing GG, Jiang L, Fuchs H, Sun TL (2009) Smart surface of water-induced superhydrophobicity. Chem Commun:2658–2660

Wang X, Ding B, Li B (2013) Biomimetic electrospun nanofibrous structures for tissue engineering. Mater Today 16:229–241

Wang Y, Lai C, Hu H, Liu Y, Fei B, Xin JH (2015) Temperature-responsive nanofibers for controllable oil/water separation. RSC Adv 5:51078–51085

Wang X, Yu J, Sun G, Ding B (2016a) Electrospun nanofibrous materials: a versatile medium for effective oil/water separation. Mater Today 19:403–414

Wang Y, Lai C, Wang X, Liu Y, Hu H, Guo Y, Ma K, Fei B, Xin JH (2016b) Beads-on-string structured nanofibers for smart and reversible oil/water separation with outstanding antifouling property. ACS Appl Mater Interfaces 8:25612–25620

Wenzel RN (1936) Resistance of solid surfaces to wetting by water. Ind Eng Chem 28:988–994

Wong TS, Sun T, Feng L, Aizenberg J (2013) Interfacial materials with special wettability. MRS Bull 38:366–371

Wu ZL, Wei RB, Buguin A, Taulemesse J, Moigne NL, Bergeret A, Wang XG, Keller P (2013) Stimuli-responsive topological change of microstructured surfaces and the resultant variations of wetting properties. ACS Appl Mater Interfaces 5:7485–7491

Xia F, Zhu Y, Feng L, Jiang L (2009) Smart responsive surfaces switching reversibly between super-hydrophobicity and super-hydrophilicity. Soft Matter 5:275–281

Xin B, Hao J (2010) Reversibly switchable wettability. Chem Soc Rev 39:769–782

Xu LY, Ye Q, Lu XM, Lu QH (2014) Electro-responsively reversible transition of polythiophene films from superhydrophobicity to superhydrophilicity. ACS Appl Mater Interfaces 6:14736–14743

Yang J, Zhang ZZ, Men XH, Xu XH, Zhu XT, Zhou XY (2011a) Counterion exchange to achieve reversibly switchable hydrophobicity and oleophobicity on fabrics. Langmuir 27:7357–7360

Yang J, Zhang ZZ, Men XH, Xu XH, Zhu XT (2011b) Thermo-responsive surface wettability on a pristine carbon nanotube film. Carbon 49:19–23

Zhang JP, Seeger S (2011) Superoleophobic coatings with ultralow sliding angles based on silicone nanofilaments. Angew Chem Int Ed 50:6652–6656

Zhang J, Li J, Han Y (2004) Superhydrophobic PTFE surfaces by extension. Macromol Rapid Commun 25:1105–1108

Zhang JL, Lu XY, Huang WH, Han YC (2005) Reversible superhydrophobicity to superhydrophilicity transition by extending and unloading an elastic polyamide film. Macromol Rapid Commun 26:477–480

Zhang XT, Jin M, Liu ZY, Tryk DA, Nishimoto S, Murakami T, Fujishima A (2007) Superhydrophobic TiO_2 surfaces: preparation, photocatalytic wettability conversion, and superhydrophobic−superhydrophilic patterning. J Phys Chem C 111:14521–14529

Zhang X, Guo Y, Zhang P, Wu Z, Zhang Z (2012) Superhydrophobic and superoleophilic nanoparticle film: synthesis and reversible wettability switching behavior. ACS Appl Mater Interfaces 4:1742–1746

Zhang C, Li P, Cao B (2015) Electrospun microfibrous membranes based on PIM-1/POSS with high oil wettability for separation of oil-water mixtures and cleanup of oil soluble contaminants. Ind Eng Chem Res 54:8772–8781

Zhu W, Feng X, Feng L, Jiang L (2006) UV-manipulated wettability between superhydrophobicity and superhydrophilicity on a transparent and conductive SnO_2 nanorod film. Chem Commun 26:2753–2755

Zhu Y, Li JM, He HY, Wan MX, Jiang L (2007) Reversible wettability switching of polyaniline-coated fabric, triggered by ammonia gas. Macromol Rapid Commun 28:2230–2236

Zhu W, Zhai J, Sun Z, Jiang L (2008) Ammonia responsive surface wettability switched on indium hydroxide films with micro- and nanostructures. J Phys Chem C 112:8338–8342